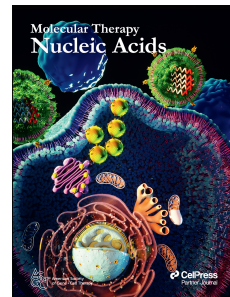


# Journal Pre-proof

Exosomal microRNAs synergistically trigger stromal fibroblasts in breast cancer.

Iolanda Scognamiglio, Lorenza Cocca, Ilaria Puoti, Francesco Palma, Francesco Ingenito, Cristina Quintavalle, Alessandra Affinito, Giuseppina Roscigno, Silvia Nuzzo, Rosario Vincenzo Chianese, Stefania Belli, Guglielmo Thomas, Timo Schomann, Alan Chan, Maria Patrizia Stoppelli, Gerolama Condorelli



PII: S2162-2531(22)00041-5

DOI: <https://doi.org/10.1016/j.omtn.2022.02.013>

Reference: OMTN 1522

To appear in: *Molecular Therapy: Nucleic Acid*

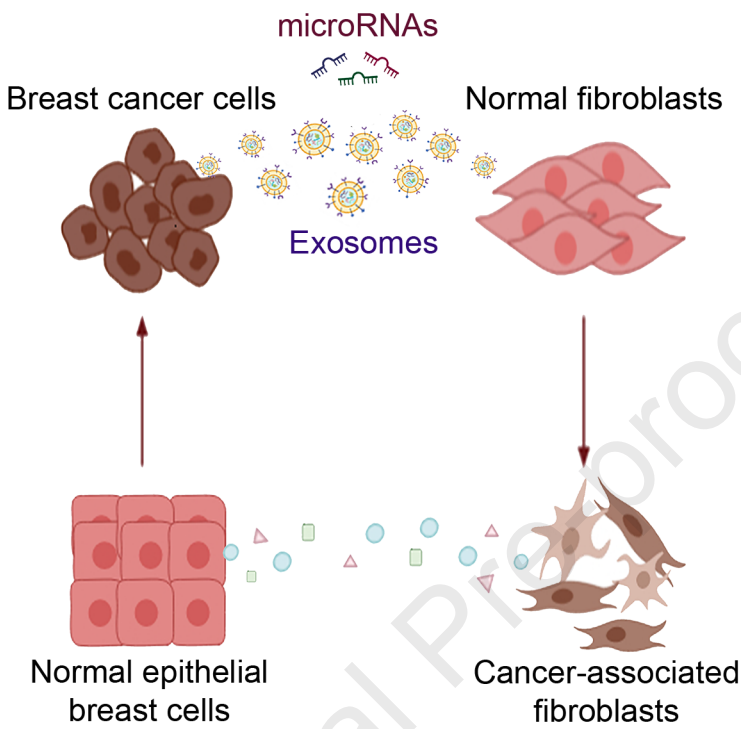
Received Date: 22 October 2021

Accepted Date: 17 February 2022

Please cite this article as: Scognamiglio I, Cocca L, Puoti I, Palma F, Ingenito F, Quintavalle C, Affinito A, Roscigno G, Nuzzo S, Chianese RV, Belli S, Thomas G, Schomann T, Chan A, Stoppelli MP, Condorelli G, Exosomal microRNAs synergistically trigger stromal fibroblasts in breast cancer., *Molecular Therapy: Nucleic Acid* (2022), doi: <https://doi.org/10.1016/j.omtn.2022.02.013>.

This is a PDF file of an article that has undergone enhancements after acceptance, such as the addition of a cover page and metadata, and formatting for readability, but it is not yet the definitive version of record. This version will undergo additional copyediting, typesetting and review before it is published in its final form, but we are providing this version to give early visibility of the article. Please note that, during the production process, errors may be discovered which could affect the content, and all legal disclaimers that apply to the journal pertain.

© 2022 The Author(s).



**TITLE PAGE**

1

2 Title:

3 **Exosomal microRNAs synergistically trigger stromal fibroblasts in breast cancer.**

4 Running title:

5 **Exosomal microRNAs trigger stromal fibroblasts.**6 Iolanda Scognamiglio<sup>1</sup>, Lorenza Cocca<sup>1</sup>, Ilaria Puoti<sup>1</sup>, Francesco Palma<sup>3</sup>, Francesco Ingenito<sup>3</sup>,  
7 Cristina Quintavalle<sup>2</sup>, Alessandra Affinito<sup>3</sup>, Giuseppina Roscigno<sup>3</sup>, Silvia Nuzzo<sup>4</sup>, Rosario  
8 Vincenzo Chianese<sup>1</sup>, Stefania Belli<sup>5</sup>, Guglielmo Thomas<sup>6</sup>, Timo Schomann<sup>3,7</sup>, Alan Chan<sup>3</sup>,  
9 Maria Patrizia Stoppelli<sup>5</sup>, and Gerolama Condorelli<sup>1,2</sup>.10 <sup>1</sup> Department of Molecular Medicine and Medical Biotechnology, University of Naples Federico  
11 II, Via Pansini 5, IT80131, Naples.12 <sup>2</sup> Institute of Endocrinology and Experimental Oncology G. Salvatore (IEOS), National Research  
13 Council (CNR), Via Pansini 5, IT80131, Naples.14 <sup>3</sup> Percuros BV, Eerbeeklaan 42, 2573 HT, Den Haag, The Netherlands.15 <sup>4</sup> IRCCS SYNLAB SDN, Via Gianturco 113, IT80143, Naples.16 <sup>5</sup> Institute of Genetics and Biophysics (IGB), National Research Council (CNR), Via Castellino  
17 111, IT80131 Naples.18 <sup>6</sup> Mediterranea Cardiocentro, Via Orazio, 2, IT80122, Naples.19 <sup>7</sup> Department of Radiology, Leiden University Medical Center, Albinusdreef, 2, 2333 ZA,  
20 Leiden, The Netherlands.

21 Correspondence should be addressed to G.C. (Via Tommaso de Amicis, 95, 80131, Naples).

22 Tel.: 0815452921. Email: [gecondor@unina.it](mailto:gecondor@unina.it))

23 This work was carried out in Naples, Italy.

24

25

26

**ABSTRACT**

27 Triple negative breast cancer (TNBC) is the most aggressive breast cancer subtype. TNBC  
28 progression is sustained by the recruitment of a strong tumor microenvironment (TME) mainly  
29 composed of Cancer-Associated Fibroblasts (CAFs) able to endorse tumor hallmarks. Increasing  
30 evidence demonstrated that exosomes mediate the crosstalk between cancer cells and TME.  
31 We examined TNBC-derived exosomes and their microRNAs (miRNAs) cargo in the activation  
32 of normal fibroblasts (NFs) towards CAFs. We demonstrated that TNBC cell-derived exosomes  
33 increased NF collagen contraction and migration alongside CAF molecular markers.  
34 Furthermore, exosome-activated fibroblasts promoted the invasion potential of normal breast  
35 epithelial cells as assessed by the organotypic co-culture assay which resembled the *in vivo*  
36 context. We further investigated TNBC cell-derived exosomes cargo in activating NFs to  
37 CAFs, by performing a small RNA-sequencing. We found that the synergistic action of  
38 miRNAs-185-5p, -652-5p, and -1246 boosted fibroblast migration and contraction abilities  
39 promoting a specific CAF sub-specialization towards a pro-migratory functional state. All  
40 together these data highlighted the role of breast cancer cells in the re-education of TME,  
41 thus contributing to tumor evolution.

42

43

44

45 Triple-negative breast cancer (TNBC) is the most aggressive breast cancer subtype;  
46 moreover, there is no molecular targeted therapy available.<sup>1</sup> TNBC is characterized by high  
47 intra-tumoral heterogeneity and plasticity that dictate multiple malignant signs, including  
48 treatment resistance and metastasis. Indeed, the rapid spread of metastases remains the  
49 main hindrance to a positive clinical outcome.<sup>2</sup> Interestingly, this aggressive attitude is  
50 encouraged by the tumor microenvironment (TME), which actively participates in all stages  
51 of tumor progression, and is now recognized as a cancer hallmark.<sup>3,4</sup> In breast cancer, the  
52 TME is composed mainly of cancer-associated fibroblasts (CAFs), which are generally  
53 derived from the surrounding stroma and can be recruited by cancer cells to endorse  
54 different tumor functions, in particular invasion and metastasis.<sup>5-8</sup>

55 Research on CAFs has grown in recent years and has been focused in particular on the  
56 distinct sub-specializations CAFs acquire during cancer enrolment.<sup>9</sup> Indeed, CAFs are the  
57 most effective cells within the TME in extracellular-matrix (ECM) remodeling due to their  
58 capacity for enzyme-mediated ECM degradation and force-dependent ECM reshuffling.<sup>10-13</sup>  
59 In this scenario, extracellular vesicles, such as exosomes, have been found to be important  
60 mediators, particularly in the crosstalk between cancer and TME through the transfer of  
61 biological molecules, such as proteins, lipids, mRNAs, and microRNAs (miRNAs), that  
62 sustain cancer development and progression.<sup>14-18</sup>

63 The dysregulation of miRNAs in cancer has been extensively described to influence cell  
64 proliferation, metastasis, angiogenesis, stem phenotype, and resistance to therapies. Thereby,  
65 miRNA profiling has been employed for cancer diagnosis, prognosis, and drug response  
66 prediction in patients.<sup>19-21</sup>

67 As an instance, tumor suppressor miR-34 family is recognized as one of the most significant  
68 in cancer being investigated in numerous pre-clinical and clinical studies<sup>22-29</sup>. Interestingly,  
69 miR-34a mimic-based drug was employed in the MRX34 clinical trial (NCT01829971), that  
70 represented the first-in-human phase 1 study of a microRNA-based cancer therapy.<sup>30</sup> Even  
71 though the clinical trial prematurely terminated, it constituted the first concrete application of  
72 miRNAs in the clinics and a solid proof-of-concept for miRNA-based cancer therapy.

73 Notably, miRNAs can be selectively loaded into the exosomes released by cancer cells, and  
74 directed to their extracellular target compartments, thus contributing to the regulation of  
75 different tumor processes, including the recruitment of cellular components from the TME.<sup>31,32</sup>

76 Here, we investigated whether TNBC-derived exosomes and their miRNA cargo may affect  
77 the conversion of fibroblasts into a CAF-like phenotype within the TME. Our results  
78 demonstrate that exosomal miR-185-5p, -652-5p, and -1246 synergistically activate stromal  
79 fibroblasts by promoting a specific pro-migratory functional state that could serve for TNBC  
80 cell migration and invasion.

**RESULTS**

81

82

83 **Breast cancer-derived exosomes are transferred to normal fibroblasts.**84 To study whether the crosstalk between breast cancer cells and surrounding fibroblasts is  
85 mediated also by exosomes, we isolated exosomes from MDA-MB-231 cells through a  
86 polymeric precipitation method (ExoQuickTC, SBI). The tumoral exosomes were then  
87 characterized by Nanoparticle Tracking Analysis (NTA), transmission electron microscopy  
88 (TEM) and western blotting analyses.89 NTA, performed with the Nanosight NS300 system equipped with a blue laser (405 nm),  
90 revealed that there was a major particle size peak at approximately 105nm, corresponding to  
91 mean diameter of exosomes (**Fig. 1a**). Western blotting revealed there was expression of the  
92 typical exosomal protein markers CD63, CD81, CD9, and Tsg101 and absence of the  
93 endoplasmic reticular protein Calnexin, indicating there was no cellular contamination (**Fig.**  
94 **1b**). Then, the morphology of exosomes was analyzed by TEM technique (**Fig. 1c**). These  
95 data confirmed the exosomal origin for isolated vesicles.96 To determine whether there was a transfer of breast cancer-derived exosomes to normal  
97 fibroblasts, we took advantage of primary stromal fibroblasts derived from surgical resection  
98 of normal breast tissues and/or fibroadenomas. Due to the benign origin of fibroadenoma, we  
99 chose to define fibroblasts isolated from this tumor by convention as normal fibroblasts (NFs).  
100 More in detail, primary fibroblast cell lines were derived from three female patients (pt. #1,  
101 #2, and #3) between 21 and 44 years of age and presenting with various clinicopathological  
102 features, including two fibroadenomas (pt. #1 and #2) and one mammary reduction (pt.#3)  
103 without any pathological signs. PKH26-labeled MDA-MB-231 cell-derived exosomes were then  
104 incubated for 12h with NFs (pt.#1) and subjected to immunofluorescence analysis. We observed  
105 that PKH26-labeled exosomes were distinctly taken up by NFs. Indeed, confocal microscopy

106 indicated co-localization of PKH26 derived from exosomes and β-Actin from NFs (**Fig. 1d**),  
107 confirming that normal fibroblasts actively took up breast cancer-derived exosomes.

108

109 **MDA-MB-231 cell-derived exosomes promote a CAF-like phenotype in NFs.**

110 Cell contractility and motility are regarded as major hallmarks of activated CAFs within the  
111 TME to foster cancer cell invasion.<sup>33-35</sup> Therefore, we assessed the effect of breast cancer-  
112 derived exosomes on fibroblast-mediated collagen contraction. To this end, NFs (pt. #1, #2,  
113 #3) were plated inside a type 1 collagen matrix and incubated with MDA-MB-231 cell-  
114 derived exosomes or PBS (control) to examine their contractile ability. After 24h, we observed  
115 that NFs cultured in the presence of exosomes reduced the collagen plug area compared to  
116 control NFs, indicating increased cell contractility mediated by exosomes (**Fig. 2a, b**).

117 Likewise, to verify whether breast cancer-derived exosomes affected the migratory potential  
118 of the fibroblasts, we pre-treated NFs (pt. #1, #2, #3) with MDA-MB-231 cell-derived  
119 exosomes or PBS for 48h and then performed a Transwell® migration assay. We found  
120 improved migration when NFs were cultured in the presence of exosomes (**Fig. 2c, d**).

121 Thereafter, to further assess the progression of NFs toward a CAF-like phenotype, the  
122 expression of molecular markers usually associated with the CAF phenotype was examined.

123 To this end, we performed quantitative real time-PCR to measure the levels of FAP, Caveolin-  
124 1, SLC16A3, and SLC2A1 mRNAs in NFs cultured with MDA-MB-231 cell-derived exosomes.

125 The presence of exosomes was associated with upregulation of these genes, a finding  
126 supporting the notion of fibroblasts being converted to a CAF-like phenotype (**Fig. 2e**).

127

128 **Exosome-activated fibroblasts induce invasion in normal breast epithelial cells.**

129 To investigate the effects of fibroblast activation within the TME, we carried out three-  
130 dimensional cell-cell interaction modeling by setting up an *in vitro* invasion organotypic assay,

131 as already reported<sup>36</sup>. NFs (pt. #3) were seeded on a type 1 collagen matrix, then cultured  
 132 in the presence of MDA-MB-231 cell-derived exosomes or PBS for 48 h to ensure fibroblast  
 133 activation. Subsequently, normal breast epithelial cells (cell line MCF10A) were seeded on  
 134 the top of the fibroblast-containing collagen matrix for 14 days, which was transferred to an  
 135 invasion grid and finally paraffin-embedded for analysis. Activation of NFs induced by the  
 136 presence of the exosomes increased the number of MCF10A cells invading the matrix, as  
 137 demonstrated by the positive Pan-cytokeratin signal from cells stained in the collagen section  
 138 (**Fig. 3a, b**). These data suggested that MDA-MB-231-derived exosomes have a pro-tumor  
 139 stromal function triggering the activation of NFs to a CAF-like phenotype. Moreover, our  
 140 organotypic assay outlined how the impact of cancer-derived exosomes on fibroblasts contribute  
 141 to malignant transformation promoting the invasive capacity of non-tumorigenic breast epithelial  
 142 cells.

143

#### 144 **miRNA expression profile of breast cancer exosomes.**

145 To investigate whether the breast cancer exosomal cargo was involved in fibroblast activation  
 146 within the TME, we performed small-RNA sequencing to identify miRNAs (miRs) differentially  
 147 expressed in NFs cultured with MDA-MB-231 cell-derived exosomes or PBS for 24h. We  
 148 found that 14 miRNAs were significantly upregulated in NFs (pt. #1) when exposed to the  
 149 exosomes (**Fig. 4a**). We then focused our attention on miR-185-5p, -652-5p, and -1246 since  
 150 they were demonstrated to be up-regulated in NFs upon MDA-MB-231-derived exosome  
 151 incubation (**Fig.4b**). Interestingly, the basal expression levels of these three miRNAs were  
 152 higher in CAFs compared to NFs (**Fig.4c**), indicating that they are involved in fibroblast  
 153 activation. Furthermore, we found that miR-185-5p, 652-5p, and -1246 were predicted to be  
 154 actively sorted into exosomes by the MDS<sup>2</sup> bioinformatics tool (<http://cse-jcui-08.unl.edu:7000/input>), previously described.<sup>37</sup> Indeed, we found short-sequence motifs  
 155 (EXOmotifs) in the three miRNAs that predicted their loading into exosomes (**Fig. 4d**). Based  
 156

157 on prediction results, we investigated whether the three miRNAs were loaded into exosomes,  
 158 by adopting an over-expression model. Hence, we transfected miR-185-5p, -652-5p, -1246,  
 159 and a Scramble sequence (as control) in MDA-MB-231 cells for 48h. Then, we isolated  
 160 exosomes and performed a q-RT-PCR to check the expression levels of the three miRs both  
 161 in cells and in the relative exosomes. Interestingly, we found that a consistent portion of  
 162 miR-185-5p, -652-5p, and -1246 were found overexpressed in MDA-MB-231-derived exosomes  
 163 (**Suppl. Fig.1**), indicating that they were loaded into exosomes. Altogether, these findings  
 164 directed us to study these three miRNAs among the other upregulated miRNAs identified by  
 165 RNA-sequencing. We then investigated whether the miRNAs shuttled via breast cancer-derived  
 166 exosomes trigger NF conversion to CAFs. We found that transfection of the individual  
 167 miRNAs had no significant biological effects on fibroblast activation, as shown by western  
 168 blot for FAP, MCT4, and Caveolin-1, known markers associated to CAF phenotype  
 169 (**Suppl.Fig.2a, b**). Therefore, we hypothesized that miR-185-5p, -652-5p, and -1246 might  
 170 work synergistically, as already reported for miR-185-5p.<sup>38</sup> Indeed, we found that combined  
 171 transfection of the three miRNAs (combo miRs) was associated with upregulated CAF markers  
 172 (FAP, MCT4, and Caveolin-1) in all three patient-derived NFs (**Fig. 4e, f**).  
 173

174 **Exosomal miR-185-5p, -652-5p, and -1246 synergistically activate fibroblasts toward a  
 175 pro-migratory functional phenotype.**

176 The main ability acquired by CAFs in the TME is ECM remodeling, a process promoting  
 177 permissive tracks for cancer cell invasion.<sup>34</sup> Coherently, the above results demonstrated that  
 178 the combo miRs mediated the activation of NFs by primarily boosting their motility in the  
 179 ECM. To further explore this, we set up a collagen contraction assay, plating NFs pre-  
 180 transfected with combo miRs or a scrambled control onto type 1 collagen matrices. We found  
 181 that the synergistic action of the three miRNAs promoted fibroblast collagen contraction, as  
 182 shown by reduction of collagen plug area in combo miRs-transfected NFs (**Fig. 5 a, b**).

183 We then investigated the invasion potential of fibroblasts, specifically their ability to move  
184 within the ECM as a result of its degradation. To this end, we transfected NFs (pt. #1, #2,  
185 #3) with combo miRs and performed a Transwell invasion assay, seeding the cells in a  
186 Matrigel solution plated on top of the migration chamber, thus simulating three-dimensional  
187 ECM. We observed increased invasion by NFs transfected with combo miRs, as demonstrated  
188 by the higher absorbance values of crystal violet eluted from migrated cells (**Fig. 5 c, d**).  
189 Considering that ECM remodeling depends on force-mediated and protease-dependent  
190 mechanisms,<sup>34</sup> we investigated integrin (ITG) and matrix metalloprotease (MMP) expression  
191 in NFs after combo miRs overexpression. For this, we conducted western blot analysis for  
192 the expression of ITGB1 and ITGA5 proteins, major players in mechanical force-mediated  
193 cell invasion and extracellular matrix modeling, especially during CAF transformation.<sup>39-42</sup> We  
194 found that ITGB1 and ITGA5 were increased in NFs transfected with combo miRs after 72h  
195 (**Fig. 5 e, f**), suggesting there was a higher driving force exerted by fibroblasts to contract  
196 the collagen matrix. However, the protease activity involved in matrix degradation is arbitrated  
197 by different members of the MMP protein family. In particular, MMP1, 2, 3, and 9 are  
198 mainly upregulated in breast cancer stroma under the influence of cancer cells.<sup>43-45</sup> We found  
199 that after 48h of transfection, combo miRs led to increased levels of MMP 1, 2, and 3,  
200 justifying the boost in fibroblast invasive potential (**Fig. 5 e, f**).  
201 Moreover, we found that combo miRs promoted a pro-migratory phenotype in NFs, as  
202 demonstrated by Transwell migration and scratch assays (**Fig. 6 a-d**). To corroborate these  
203 results, we investigated expression of FAK, the main regulator of focal adhesion turn-over  
204 responsible for cell movement.<sup>46</sup> We found upregulation of the activated form of FAK protein  
205 (phosphorylated at Y576/577) using western blot analysis (**Fig. 6 e, f**) in NFs (pt.#1, #2, #3)  
206 transfected with combo miRs, indicating an activation of the molecular pathway involved in  
207 cell migration. All together, these data demonstrated that miR-185-5p, miR-652-5p, and miR-  
208 1246 synergistically foster a pro-migratory functional state in NFs within the TME.

209

## DISCUSSION

210

211 The data presented here shed light on the role of exosomes in the crosstalk between the  
212 TME and breast cancer cells. Our results strengthen knowledge on the mechanisms adopted  
213 by breast cancer to potentiate the oncogenic phenotype of neighboring cells within the TME.  
214 Indeed, we demonstrate that TNBC-derived exosomes and the miRNA cargo they hold activate  
215 stromal fibroblasts to obtain a specific pro-migratory functional phenotype, so potentially  
216 enabling tumor invasion and metastasis.

217 It is known that fibroblasts are recruited by cancer cells within the TME to support different  
218 tumor traits.<sup>7,47</sup> However, the major obstacle in studying CAFs is high functional heterogeneity  
219 and lack of specific molecular markers defining their status, even considering occasional  
220 antitumorigenic roles.<sup>9</sup> However, some researchers have tried to associate precise gene  
221 signatures to CAF subtypes.<sup>48</sup> In our case, fibroblast activation mediated by cancer cell  
222 exosomal miRNAs was associated with upregulation of MCT4, FAP, and Caveolin-1, among  
223 other canonical CAF markers. The role of Caveolin-1 in CAF activation is controversial. In  
224 fact, some studies have demonstrated that loss of Caveolin-1 expression is a trait associated  
225 with CAF transformation.<sup>49-51</sup> In contrast, our data are in line with those of Jacky G. Goetz  
226 *et al.* showing that the presence of Caveolin-1-enriched CAFs correlates with tumor invasion  
227 and metastasis by promoting the biomechanical remodeling of tumoral stroma.<sup>13</sup>

228 In the context of breast cancer TME, intracellular and extracellular miRNAs have been widely  
229 reported to mediate the cross-talk between CAFs and cancer cells.<sup>52-58</sup> In this manuscript, we  
230 provided evidence supporting the notion that breast cancer cell exosomal miRNAs induce a  
231 CAF-related pro-migratory phenotype, rather than a proliferative pro-survival one. Indeed, any  
232 significant effect on the activation of proliferative and survival pathways mediated by combo  
233 miRs was observed (**Suppl.Fig.3 a, b**), as shown by cell viability assay and western blotting  
234 for phosphorylated AKT (S473) and phosphorylated β-catenin (S33/37/T41), known markers

235 of cell proliferation, self-renewal, and survival in cancer.<sup>59-62</sup> In contrast, delivery to fibroblasts  
236 of the breast-cancer cell exosomal combo miRs induced the former to increase migration,  
237 contraction, and invasion, all characteristics acquired by specific CAF subtypes. Otherwise,  
238 the incubation of NFs with MCF10A-derived exosomes, that presented lower levels of two  
239 of the three miRs, showed no effect on fibroblast migration, indicating the presence of a  
240 specific mechanism related to the combined exosomal miRs function (**Suppl. Fig.4 a, b**).  
241 Moreover, the overexpression in fibroblasts of combo miRs induced the expression of MMPs  
242 (type 1, 2, and 3) and ITGs ( $\alpha 5$  and  $\beta 1$  subunits) and increased FAK phosphorylation  
243 (Y576/577), components of major pathways involved in cancer cell invasion and motility,  
244 since they operate in protease-dependent ECM remodeling and cellular movement.<sup>40,54,63</sup>  
245 Although breast cancer prognosis has been improved by the development of molecular targeted  
246 therapies, the treatment of TNBC is still a challenge due to its highly invasive nature and  
247 relatively low response rate. These adverse clinicopathological aspects are often caused by  
248 CAFs populating the activated tumoral stroma and the exosomal cargo shed by cancer cells  
249 into the surrounding TME.<sup>64-66</sup> Thus, discovering new molecular targets for TNBC prognosis  
250 and drug response prediction has become fundamental. Regarding this point, our study shows  
251 that three exosomal miRNAs (miR-185-5p, miR-652-5p, and miR-1246) act synergistically to  
252 promote fibroblast transformation in the context of TNBC.  
253 MiR-185-5p has already been reported in patients with severe active alopecia to work in  
254 synergy with other miRNAs rather than alone,<sup>38</sup> a finding coherent with our initial hypothesis.  
255 Furthermore, upregulation of this miRNA has been observed specifically in lymph nodes with  
256 metastases from breast cancer; similarly, it has emerged as a prognostic factor of radiation-  
257 related toxicity in the serum of patients with oropharyngeal cancer,<sup>67</sup> and as a predictive  
258 biomarker of chemotherapy response and metastasis formation in colorectal and gastric  
259 cancer.<sup>68,69</sup>

260 Likewise, miR-652-5p has been reported upregulated in breast malignancies. However,  
261 decreased expression of this miRNA has been correlated with esophageal carcinoma progression  
262 and recurrence.<sup>70,71</sup> This difference could be explained by the fact that miRNAs can operate  
263 in different ways depending on the biological system they are acting in.

264 Regarding miR-1246, this is a well know master regulator in cancer. In particular, its  
265 upregulation has been associated with tumor growth, metastasis, and drug resistance in different  
266 types of cancer.<sup>72-74</sup> In breast cancer, exosomal miR-1246 has been used as diagnostic  
267 biomarker due to its high expression specificity.

268 Given the considerable role of these miRNAs in cancer, the novelty of our study lies in the  
269 combined effect exerted by these exosomal miRNAs on fibroblast activation within the TME.  
270 This could reflect the existence of a specific miRNA profile in the tumor cells' exosomal  
271 cargos, with a well-defined scope of action.<sup>75</sup>

272 Altogether, our results demonstrate that exosomes encourage breast cancer development by  
273 delivering specific miRNAs that stimulate the formation of a singular and aggressive TME.  
274 These findings may aid the development of novel, alternative strategies for TNBC theragnostic.  
275 Better comprehension of the mechanisms underlying the behavior of CAFs within the context  
276 of a tumor may help to adapt them for specific clinical benefits.

277

**MATERIALS AND METHODS**

278

279 **Primary and continuous cells cultures.**

280 Primary cultures of fibroblasts (NFs) were obtained from patients undergoing breast reduction  
281 surgery from Clinica Mediterranea (Naples, Italy). Patients' informed consent was obtained  
282 before sample collection. This study was conducted according to the criteria set by the  
283 declaration of Helsinki and approved by the Research Ethics Committees of the University  
284 of Naples Federico II (n° 119/15ES1) and of "A.S.L. Napoli 1" (n°247/C.E.-20/2021Oss).  
285 Briefly, human breast specimens were cut by mechanical fragmentation with sterile blades  
286 and tongs. Extracellular matrix was digested with collagenase (Sigma-Aldrichm) for 2h under  
287 continuous agitation (200 rpm) at 37°C. Then, the cellular suspension was differentially  
288 centrifuged to separate epithelial cells from fibroblasts population (200 rpm for 2 minutes to  
289 obtain a pellet of epithelial cells and 1300 rpm for 5 minutes to obtain fibroblast population).  
290 Fibroblasts were grown in Dulbecco's Modified Eagle's Medium/Nutrient F12-Ham  
291 (DMEMF12 – Sigma Aldrich, Cod. D8437, lot. #RN BG9065) supplemented with 10% heat-  
292 inactivated fetal bovine serum (FBS, Sigma-Aldrich, Cod. F7524, Lot. #BCBW0228), 1%  
293 penicillin/streptomycin (A/A, Gibco, Cod. 15240-062, Lot. #2321085), 1% amphotericin B  
294 (Gibco, NY-USA, Cod. 15290-026, Lot #2244434) at 37°C with 5% CO<sub>2</sub>. Breast cancer  
295 continuous cell line MDA-MB-231(ATCC) was grown in RPMI-1640 medium (Sigma-Aldrich,  
296 Cod. R8758, Lot. #RNBF0094) supplemented with 10% heat inactivated FBS, 1% A/A.  
297 Normal Breast Epithelial cell line MCF-10A (ATCC) was cultured in DMEM-F12  
298 supplemented with 5% heat-inactivated fetal horse serum, 1% of A/A, 1% amphotericin B  
299 and with all hormones and factors needed for their growth: EGF (1µg/µl), hydrocortisone  
300 (1µg/µl), cholera toxin (100µg/µl), insulin (20µg/µl). All media and supplements were from  
301 Sigma-Aldrich (Milan, Italy).

302

303

304 **Exosome Isolation**

305 Exosomes were isolated from cell culture media of MDA-MB-231 cells. In detail, 4x10<sup>6</sup> cells  
306 were plated in 150mmx25mm cell culture dishes (Corning, #430599) with their usual growth  
307 medium (described in the previous section) to allow plate attachment. After 24h, cells were  
308 washed twice with PBS (Dulbecco's Phosphate Buffered Saline, Sigma-Aldrich, Cod. D8537,  
309 Lot. #RNBH3372) and 12 ml of RPMI medium (Sigma-Aldrich) supplemented with 10%  
310 Exo-FBS (FBS depleted of exosomes, SBI, System Biosciences, Cod. EXO-FBS-250A-1, Lot.  
311 #161004-002), 1% of A/A and 1% amphotericin B was added. After 48h, culture media were  
312 collected and centrifuged at 3000 g for 15 minutes RT to remove cellular debris. The  
313 supernatants were transferred into new sterile tubes and the appropriate volume of the  
314 ExoQuick-TCTM Exosome Isolation Reagent (SBI, System Biosciences, Cod. EXOTC50-A)  
315 was added according to manufacturers' instructions. Then, tubes were gently mixed until the  
316 separation between the two phases was no longer visible. Tubes were kept standing at 4°C  
317 O/N. The following day, tubes were centrifuged first at 1500 g for 30 minutes, and then at  
318 1500 g for 5 minutes to ensure the complete removal of the ExoQuick-TCTM solution. Lastly,  
319 exosome pellets were resuspended in 300 µl of PBS solution.

320

321 **Nanoparticle tracking analysis**

322 Exosome size and particle number were analyzed using the NS300 nanoparticle characterization  
323 system (NanoSight, Alfatest – Rome, Italy) equipped with a blue laser (405 nm). In brief,  
324 40 µl of exosome isolation (see “Exosome Isolation” section) was diluted with PBS to a  
325 final volume of 400µl and loaded into the instrument. For the measurement, the instrument

326 software (NTA 3.1 Build 3.1.54) was used under the following settings. Capture settings:  
327 Camera type: sCMOS; Camera level: 15; Slider shutter: 1206; Slider gain: 366; FPS: 25.0;  
328 Number of frames: 1498; Temperature: 24.6-24.7°C; Viscosity (water): 0.895-0.897 cP; Dilution  
329 factor: 2 x 10e2; Syringe pump speed: 20. Analysis settings: Detect threshold: 5; Blur size:  
330 auto; Max jump distance: auto (12.3-12.9 pix). Sample measurement was performed in  
331 triplicate.

332

### 333 **Transmission electron microscopy**

334 TEM imaging was carried out at the Department of Radiology of Leiden University Medical  
335 Center (Leiden, The Netherlands). Carbon-coated grids (Formvar/Carbon on 200 Mesh Copper;  
336 AGS162; Van Loenen Instruments; Zaandam, the Netherlands) were glow-discharged for 1  
337 minute at 2x10<sup>-1</sup> mbar and 20 mA using the Emitech K950X Turbo Evaporator (Quorum  
338 Technologies; Ashford, UK). Afterwards, 3 µl of sample solution was transferred to the glow-  
339 discharged grid and left for 1 min to adhere. Excess liquid was blotted onto filter paper, and  
340 3 µl of 2% uranyl acetate in distilled water was applied to the grid for negative staining.  
341 Excess uranyl acetate was removed by blotting after 1 min, and the sample was air-dried for  
342 10 min. Grids were placed on a room temperature holder and observe at a voltage of 120  
343 kV with a Tecnai 12 Twin (FEI Company; Oregon, USA) fitted with a OneView Camera  
344 Model 1095 (Gatan; Pleasanton, USA). DigitalMicrograph 3.4 was used to capture and save  
345 digital images (Gatan).

346

### 347 **Cell transfection and exosome treatment**

348 NFs (2,5 x10<sup>5</sup>) were seeded in 60mm x 15mm cell culture dishes (Corning Incorporated,  
349 #353004) and the combination of pre-miR miRNA precursor-185-5p, pre-miR-652-5p, and pre-

350 miR-1246 (combo miRs), as well as pre-mir-Scramble (Ambion, Life technologies Milan Italy)  
351 were transiently transfected at the final concentration of 150µM for each transfection point  
352 by using Oligofectamine™ Reagent (Invitrogen, Thermo Fisher Scientific – Milan, Italy- Cod.  
353 12252-011, Lot. #2030861) in a reduced serum condition (Opti-MEM, Gibco, Cod. 31985-  
354 047, Lot. #2091581). After 4h, cell medium was supplemented with a final concentration of  
355 10%FBS to restore optimal cell growth conditions. Cells were collected at 24h, 48h, and/or  
356 72h of transfection for downstream analysis or applications. Exosomes isolated from MDA-  
357 MB-231 were quantized using Bradford reagent (Protein assay dye-Bio- Rad, Cod. 5000006,  
358 Lot. # 64254929) and a total amount of 40ug was used for NFs treatments. Briefly, NFs  
359 ( $2,5 \times 10^5$ ) were seeded in p60mm dishes in 10% FBS-DMEM-F12 as long as they get attached,  
360 then washed twice with PBS solution and kept in DMEM-F12 medium supplemented with  
361 10% Exo-FBS for the exosome treatment. Lastly, NFs were collected after 24h and/or 48h  
362 for downstream analysis.

363

#### 364 **Exosome labeling and immunofluorescence assay**

365 Exosomes isolated from MDA-MB-231cells (see “Exosome isolation and characterization”  
366 section) were labeled with the red fluorescent cell membrane linker PKH26 (Sigma-Aldrich,  
367 #SLBT6344). Briefly, exosomes (40 µg) were stained with PKH26 (0,33 µl) for 5 minutes  
368 in dark at RT in a final reaction volume of 2ml. Then, the same amount of 1% BSA (2  
369 ml) was added to stop the labelling reaction. Finally, samples were ultracentrifuged (Beckman  
370 coulter, Optima MAX) twice at 100,000 g for 70 minutes at 4°C, and pellets were resuspended  
371 in 500µl of PBS. For the immunofluorescence assay,  $5 \times 10^5$  NFs were plated on glass  
372 coverslips in a 24 multiwell plate. The following day, NFs were treated with PKH26-labelled  
373 exosomes for 12h, then washed three times with PBS and finally fixed with MetOH/Acetone  
374 1:1 for 10 minutes at -20°. After 3 washes in PBS, cells were blocked in 1% PBS-BSA

375 with 0.3% Triton X-100 (SIGMA-ALDRICH, cat. # 9002-93-1) solution at RT for 15 minutes.  
376 Subsequently, cells were stained with anti- β-Actin primary antibody (1:1000) diluted in  
377 blocking solution for 1 hour at RT for cytoskeleton detection. After 3 washes in PBS, the  
378 secondary antibody Goat Anti-Mouse IgG-FITC (Santa Cruz Biotechnology, #F0211-1:300 in  
379 PBS) was added for 30 minutes at RT. Lastly, cells were incubated with DAPI (BD  
380 Pharmingen™, Cat.564907 1:1000 in PBS) for 10 minutes at RT in dark for nuclei visualization.  
381 Coverslips were washed and mounted with 2µl of 1:1 Glycerol (Sigma-Aldrich, #114K0183V)  
382 in PBS on a microscope slide and images from confocal microscopy (Leica LSM700) were  
383 taken and analyzed to check exosomes uptake.

384

### 385 Protein isolation and Western Blotting

386 Cells were washed twice in ice-cold PBS and exosomes previously isolated were lysed in JS  
387 buffer (50 mM HEPES pH 7.5 containing 150mM NaCl, 1% Glycerol, 1% Triton X100,  
388 1.5mM MgCl<sub>2</sub>, 5mM EGTA, 1 mM Na<sub>3</sub>VO<sub>4</sub>, and 1X protease inhibitor cocktail). Protein  
389 concentration was determined by the Bradford reagent (Protein assay dye-BioRad, Cod.  
390 5000006, Lot. # 64254929) using bovine serum albumin as the standard, and equal amounts  
391 of proteins were analyzed by SDS-PAGE (12.5% acrylamide Bio-Rad, Cod. 1610158, Lot.  
392 #64269544). First, gels were electroblotted into nitrocellulose membranes (GE Healthcare Life  
393 Science, cat. #10600002); then, membranes were blocked for 1h with 5% blotting-grade  
394 blocker (Bio-Rad, #1706404) in Tris Buffered Saline (TBS- Bio-Rad, #1706435) containing  
395 0.1% Tween-20 (SIGMA-ALDRICH, Co., #P1379-1L), and finally incubated at 4°C over night  
396 with the primary antibodies. Signal detection was performed by peroxidase-conjugated  
397 secondary antibodies using the enhanced chemiluminescence system (Thermofisher, Milan  
398 Italy). Primary antibodies used were: anti-FAP (Abcam, UK, ab53066- 1:1000 in 5% TBS-  
399 milk), anti-Caveolin-1 (Santa Cruz Biotechnologies, MA, USA, sc-53564 -1:500 in 5% TBS-

400 BSA), anti-MCT4 (Santa Cruz Biotechnologies, MA, USA, sc-376140-1:500 in 5% TBS-BSA),  
401 anti-β-ACTIN (Signa, USA, A5441-1:15000 in 5% TBS-milk), anti-phospho-FAK(Y576/577)  
402 (Cell signaling technology, #3281- 1:500 in 5% TBS-BSA), anti-FAK(Cell signaling  
403 technology, #71433-1:1000 in 5% TBS-milk), anti-CD63 (Santa Cruz Biotechnologies, MA,  
404 USA,sc-15363-1:500 in TBS-milk), anti-TAPA1(Abcam, UK, ab35026- 1:1000 in 5% TBS-  
405 milk), anti-Tsg101(Abcam, UK,ab83- 1:1000 in 5% TBS-milk), anti-Hsp70 (Santa Cruz  
406 Biotechnologies, MA, sc-32239-1:500 in 1:1000 in 5% TBS-milk), anti-Calnexin (Abcam, UK,  
407 ab10286-1:1000 in 5% TBS-milk), anti MMP1 (Santa Cruz Biotechnologies, MA, USA, sc-  
408 21731, 1:500 in 5% TBS-milk), MMP2 (Santa Cruz Biotechnologies, MA, USA, sc-21731,  
409 1:250 in 5% TBS-milk), MMP3 (Santa Cruz Biotechnologies, MA, USA, sc-21731, 1:500 in  
410 5% TBS-milk), anti-Integrin α5 (Santa Cruz Biotechnologies, MA, USA, sc-13547, 1:500 in  
411 5% TBS-milk), and anti-Integrin β1 (Santa Cruz Biotechnologies, MA, USA, sc-13547, 1:1000  
412 in 5% TBS-milk); anti-AKT (Cell Signaling Technology, Inc., #9272, 1:1000 in 5% TBS-  
413 milk); anti-phospho-AKT. (Ser473)(Cell Signaling Technology, Inc, #9271 1:1000 in 5% TBS-  
414 milk); anti-β-Catenin (Cell Signaling Technology, Inc, #9582 1:1000 in 5% TBS-BSA); anti-  
415 phospho-β-Catenin (Ser33/37/Thr41); (Cell Signaling Technology, Inc, #9561 1:1000 in 5%  
416 TBS-BSA).

#### 417 RNA extraction and Real Time PCR

418 Total RNA (miRNAs and mRNA) was extracted using TRIZOL reagent (Life technologies,  
419 #15596018, Milan, Italy). Reverse transcription was performed starting from equal volume of  
420 total RNA/sample (150-300 ng) using miScript reverse Transcription Kit (QIAGEN, cat  
421 #218161) for total miRNAs, and SuperScript® III First-Strand (Invitrogen, cat. #18080051)  
422 for mRNAs. Quantitative analysis of miR-185-5p, miR-652-5p, miR-1246 e and RNU6A (as  
423 an internal reference) was performed by Real Time PCR using miScript SYBR Green PCR  
424 Kit (QIAGEN, cat. #218075) and miScript Primer Assays (QIAGEN, cat. #3406126). The

425 reaction for detection of miRs was performed as follows: 95°C for 15, 40 cycles of 94°C  
426 for 15'', 55°C for 30'', and 70°C for 30''. For the mRNA amplification of FAP, Caveolin-  
427 1, SLC16A3, SLC2A1, and β-Actin as internal normalizer gene we performed a Real Time  
428 PCR with iTaq™ Universal SYBR® Green Supermix (Bio-Rad, cat. #1725124) and custom-  
429 made primers for mRNAs (IDT, Milan, Italy) and. The reaction for the detection of mRNAs  
430 was performed as follows: 95°C for 15', 40 cycles of 94°C for 15'', 58°C for 30'', and  
431 72°C for 30'. All reactions were run in triplicate.

432

### 433 **Collagen contraction assay**

434 Collagen contraction assay was performed with NFs in 35mmx 10mm cell culture dishes  
435 (Corning Incorporated, #430165) for exosome treatment and in 12-well plates (Corning  
436 Incorporated, #3513) for combo miRs transfection. Type-1 collagen (Corning, #354236-33ng/μl)  
437 was resuspended in acidic environment composed of Acetic Acid (5mM) and Minimum  
438 Essential Medium Eagle (Sigma, MO275, 10X); then NaOH (1M) was added drop by drop  
439 to restore the neutral pH for cell resuspension. For contraction assay performed with combo  
440 miRs, NFs were previously transfected with combo miRs (scrambled for control) for 48h and  
441 then used for contraction assay; whereas for exosomes, NFs were first pleated in the collagen  
442 plug and then treated with exosomes. In both cases,  $1,5 \times 10^5$  NFs resuspended in 250μl of  
443 FBS were added to type-1 collagen mix prepared before. All steps during collagen handling  
444 must be performed on ice to avoid early collagen solidification. After that, plates containing  
445 collagen plugs and cells were taken at 37°C with 5%CO<sub>2</sub> for 3h to allow collagen solidification.  
446 Subsequently, collagen plugs were detached from plate walls to allow cell contraction and  
447 DMEM-F12 FBS- free medium (with or without exosomes, depending on the experiment)  
448 was added. Images of entire collagen plugs were taken after 24h with the camera tool of a  
449 mobile phone held in a fixed position. Then, plug areas were calculated with ImageJ software

450 and analyzed to check NFs contraction ability after exosomes treatment or combo miRs  
451 transfection.

452

453 **3D Organotypic coculture assay**

454 NFs were starved in DMEM F12 media without FBS for 24 h and then seeded in 35mmx  
455 10mm cell culture dishes (Corning Incorporated, #430165) in a neutralized matrix made of  
456 type- 1 collagen either treated with MDA-MB-231-derived exosomes (or PBS as control) to  
457 ensure their activation (the same procedure described in “Contraction assay” section).  
458 Additionally,  $1 \times 10^5$  MCF10A cells were seeded on the top of the collagen plug for 48h.  
459 Then, plugs were transferred to an invasion grid (Screens for CD-1 size 40 mesh, SIGMA-  
460 ALDRICH) in a 60 mm plate and complete growth medium was added underneath in order  
461 to create an air/liquid interface to trigger epithelial cell invasion. After 14 days, matrices  
462 were fixed, paraffin embedded and cut into 10 $\mu$ m sections. Organotypic matrices were stained  
463 with anti-pan cytokeratin (Santa Cruz Biotechnologies, MA, USA, sc-8018- 1:400 in blocking  
464 solution) O.N. at 4°C and then with the secondary antibody ALEXA594-conjugated goat anti-  
465 mouse (Abcam, ab150116- 1:400 in blocking solution) for 1h at RT in the dark. Images were  
466 taken either with an inverted microscope and with a fluorescent one. Number of Pan-  
467 cytokeratin positive cells was counted by ImageJ software in different fields of the images  
468 to quantify the number of invading cells.

469

470 **Transwell® - Migration assay**

471 Migration assay was carried out with 8.0  $\mu$ m polycarbonate membrane permeable 6.5 mm  
472 Transwell® inserts (Corning Incorporated, NY, USA – Cod. 3422, Lot. #11619021). NFs  
473 pretreated with exosomes (40  $\mu$ g) or transfected with miRNAs (as described in “Cell

474 transfection and exosome treatment” section) were harvested with a trypsin-EDTA solution  
475 (Sigma Aldrich, USA – Cod. T4D49 – Lot. #SLCH3365) and counted with Neubauer’s  
476 chamber. Then,  $1,0 \times 10^5$  cells were washed with PBS to remove any FBS residues,  
477 resuspended in DMEM-F12 FBS free medium, and seeded in the upper part of the Transwell®  
478 chamber. The lower part of the chamber was filled with 600  $\mu\text{L}$  of DMEM-F12 medium  
479 supplemented with 10% FBS, 1% of A/A and 1% amphotericin B to create the chemical  
480 gradient needed for cell migration. Cells were incubated at 37 °C with 5% CO<sub>2</sub> for 24 h.  
481 Subsequently, the Transwell® chambers were stained and fixed with 0.1% Crystal Violet in  
482 25% methanol for 20 minutes at RT in dark. The reaction was stopped with water and non-  
483 migrated cells were scraped off the top of the chamber with a cotton swab. Representative  
484 images were taken with the contrast phase microscopy (Leica DMI3000 B). The percentage  
485 of migrated cells was calculated by eluting Crystal Violet with 600  $\mu\text{l}$  of 1% SDS for each  
486 well and measuring the respective absorbance at 490 nm with MULTISKAN FC plate reader  
487 (Thermo Scientific).

488

489 **Invasion assay**

490 In vitro invasion assay was performed in 24-well Corning Multiwells, with 8.0  $\mu\text{m}$   
491 polycarbonate membrane permeable 6.5 mm Transwell® inserts (Corning Incorporated, NY,  
492 USA – Cod. 3422, Lot. #11619021). NFs ( $1.2 \times 10^5$ ). NFs previously transfected with combo  
493 miRs for 24h were resuspended in a mix containing Matrigel® Matrix Basement Membrane  
494 (Corning, NY – USA, Cod. 354230, Lot. #6207017) diluted 1:5 in DMEM-F12 FBS free.  
495 The lower part of the chamber was filled with 600 $\mu\text{l}$  of DMEM-F12 medium supplemented  
496 with 10% FBS, % antibiotic-antimycotics and 1% of amphotericin B to create the chemical  
497 gradient for cell movement. Cells were incubated at 37°C with 5% CO<sub>2</sub> for 72h. The  
498 Transwell® supports were stained and fixed with 0.1% Crystal Violet in 25% methanol for

499 20 minutes at RT in dark. The reaction was stopped with water, and non-migrated cells  
500 together with residual Matrigel® solution were scraped off the top of the Transwell® with a  
501 cotton swab. Representative images were taken with a contrast phase microscopy (Leica  
502 DMI3000 B). The percentage of migrated cells was evaluated by eluting Crystal Violet with  
503 600µl of 1% SDS for each well and measuring the respective absorbance at 490 nm with  
504 MULTISKAN FC plate reader (Thermo Scientific).

505

#### 506 **Scratch assay**

507 NFs ( $5 \times 10^4$ ) were seeded in a 12-well plate (Corning Incorporated, #3513) and the following  
508 day transfected with miR 185-5p, 652-5p, 1246 or with scrambled sequence as control. After  
509 48h, cells were starved for 3h in DMEM F12 FBS-free culture media. Next, a scratched  
510 wound was scraped with a 200-µL tip in each well and then cells were continuously grown  
511 in DMEM-F12 culture media complemented with 10% FBS and 1% A/A for 24h. Microscopy  
512 images were taken in different fields of the wound at the scratch moment ( $t_0$ ) and after 24h  
513 ( $t_{24}$ ) using a 5x objective of an inverted microscope (Leica DMI3000 B, Leica, Milan, Italy).  
514 Scratch area was calculated with ImageJ software and analyzed to measure the wound healing  
515 ability of NFs after combo miRs transfection.

#### 516 **RNA Sequencing**

517 NFs ( $5 \times 10^5$ ) were plated in 100mm dishes with DMEM-F12 culture media supplemented  
518 with 10% Exo-FBS (SBI, System Biosciences) and 1% A/A and treated with 120µg of MDA-  
519 MB-231 derived exosomes and the same volume of PBS solution as control. After 24 hours,  
520 cells were collected and RNA was extracted using TRIZOL reagent (Life technologies,  
521 #15596018, Milan, Italy). Samples were sent to Genomix4Life S.r.l (Baronissi, Salerno, Italy)

522 that performed Small-RNA-sequencing by using Illumina HiSeq2500 (SmallRNA 1X20M Cod.  
523 G4L1630 – iMir, Cod. G4L15055) and the bioinformatics analysis (PCA component and  
524 differentially expression analysis). Two biological replicates for each experimental point were  
525 analyzed. For the statistical analysis p. value < 0.05 alone was considered for the experimental  
526 significance; no p value adjustment was performed because of the small sample size analyzed  
527 (NFs pt.#1).

528

### 529 **In vitro cell viability assay**

530 Cell viability was evaluated with the CellTiter 96 AQueous One Solution Cell Proliferation  
531 Assay (Promega, Milan, Italy), according to the manufacturer's protocol. After 30 min. of  
532 incubation, the plates were analyzed on a Multilabel Counter (Bio-Rad, Milan, Italy) to  
533 measure the absorbance values used for the analysis.

534

### 535 **Data availability**

536 RNA-sequencing data discussed in this publication have been deposited in NCBI's Gene  
537 Expression Omnibus (Edgar et al., 2002) and are accessible through GEO Series accession  
538 number GSE185654 (<https://www.ncbi.nlm.nih.gov/geo/query/acc.cgi?acc=GSE185654>).

539

540

**AKNOWLEDGMENTS**

541 This work was supported by grants to GC from Associazione Italiana Ricerca sul Cancro  
542 AIRC (IG 2016 N. 18473), POR Campania FESR 2014-2020 “SATIN”, and Earlier Foundation  
543 to G.C. This work has received funding from the European Union’s Horizon 2020 research  
544 and innovation programme under the Marie Skłodowska-Curie projects: cONCReTE (872391),  
545 PRISAR2 (872860), CANCER (777682), PAVE (861190), and CAST (857894). G.R. is  
546 recipient of a European GRANT BARRICADE (IF\_MSCA n: 895151). A.A. is recipient of  
547 a European GRANT GLEXO (IF MSCA n:891551).

548

**AUTHOR CONTRIBUTIONS**

549

550 Conceptualization: I.S., L.C., I.P., C.Q.; Data Curation: I.S., L.C.; Formal Analysis: I.S., L.C.;  
551 C.Q.; Funding acquisition: G.C.; Investigation: I.S., L.C.; Methodology: I.S., L.C., I.P., F.P.,  
552 F.I., M.P.S., S.B., A.A., G.R., S.N., R.V.C., T.S.; Project administration: G.C., I.S.; Resources:  
553 R.T.; Software: I.S., L.C., C.Q., A.A.; Supervision: G.C.; Validation: I.S., L.C., I.P.;  
554 Visualization: I.S., L.C.; Writing- original draft: I.S., L.C.; Writing-review& editing: G.C.,  
555 F.I., F.P., G.R., M.P.S., A.A. All the authors have seen and approved the manuscript and its  
556 contents.

557

**DECLARATION OF INTERESTS STATEMENT**

558 The authors declare that they have no conflict of interest.

Journal Pre-proof

559

**Keywords**

560

561

562

563 CAF, Exosomes, miRs, TME, TNBC, Cancer, Breast Cancer, BC

564

565

566

567

568

569

570

571

572

573

574

575

576

577

## REFERENCES

- 579 1. Dent, R., Trudeau, M., Pritchard, K.I., Hanna, W.M., Kahn, H.K., Sawka, C.A., Lickley, L.A., Rawlinson,  
 580 E., Sun, P., and Narod, S.A. (2007). Triple-negative breast cancer: clinical features and patterns of  
 581 recurrence. *Clinical cancer research : an official journal of the American Association for Cancer  
 582 Research* 13, 4429-4434. 10.1158/1078-0432.CCR-06-3045.
- 583 2. Karaayvaz, M., Cristea, S., Gillespie, S.M., Patel, A.P., Mylvaganam, R., Luo, C.C., Specht, M.C.,  
 584 Bernstein, B.E., Michor, F., and Ellisen, L.W. (2018). Unravelling subclonal heterogeneity and  
 585 aggressive disease states in TNBC through single-cell RNA-seq. *Nature communications* 9, 3588.  
 586 10.1038/s41467-018-06052-0.
- 587 3. Hanahan, D., and Weinberg, R.A. (2011). Hallmarks of cancer: the next generation. *Cell* 144, 646-674.  
 588 10.1016/j.cell.2011.02.013.
- 589 4. Balkwill, F.R., Capasso, M., and Hagemann, T. (2012). The tumor microenvironment at a glance. *Journal of cell science* 125, 5591-5596. 10.1242/jcs.116392.
- 590 5. Orimo, A., Gupta, P.B., Sgroi, D.C., Arenzana-Seisdedos, F., Delaunay, T., Naeem, R., Carey, V.J.,  
 591 Richardson, A.L., and Weinberg, R.A. (2005). Stromal fibroblasts present in invasive human breast  
 592 carcinomas promote tumor growth and angiogenesis through elevated SDF-1/CXCL12 secretion. *Cell*  
 593 121, 335-348. 10.1016/j.cell.2005.02.034.
- 594 6. Toullec, A., Gerald, D., Despouy, G., Bourachot, B., Cardon, M., Lefort, S., Richardson, M., Rigaill, G.,  
 595 Parrini, M.C., Lucchesi, C., Bellanger, D., et al. (2010). Oxidative stress promotes myofibroblast  
 596 differentiation and tumour spreading. *EMBO molecular medicine* 2, 211-230.  
 597 10.1002/emmm.201000073.
- 598 7. Erdogan, B., and Webb, D.J. (2017). Cancer-associated fibroblasts modulate growth factor signaling  
 599 and extracellular matrix remodeling to regulate tumor metastasis. *Biochemical Society transactions*  
 600 45, 229-236. 10.1042/BST20160387.
- 601 8. Eiro, N., Gonzalez, L.O., Fraile, M., Cid, S., Schneider, J., and Vizoso, F.J. (2019). Breast Cancer Tumor  
 602 Stroma: Cellular Components, Phenotypic Heterogeneity, Intercellular Communication, Prognostic  
 603 Implications and Therapeutic Opportunities. *Cancers* 11. 10.3390/cancers11050664.
- 604 9. Sahai, E., Astsaturov, I., Cukierman, E., DeNardo, D.G., Egeblad, M., Evans, R.M., Fearon, D., Greten,  
 605 F.R., Hingorani, S.R., Hunter, T., Hynes, R.O., et al. (2020). A framework for advancing our  
 606 understanding of cancer-associated fibroblasts. *Nature reviews. Cancer* 20, 174-186.  
 607 10.1038/s41568-019-0238-1.
- 608 10. Kechagia, J.Z., Ivaska, J., and Roca-Cusachs, P. (2019). Integrins as biomechanical sensors of the  
 609 microenvironment. *Nature reviews. Molecular cell biology* 20, 457-473. 10.1038/s41580-019-0134-  
 610 2.
- 611 11. Hooper, S., Gaggioli, C., and Sahai, E. (2010). A chemical biology screen reveals a role for Rab21-  
 612 mediated control of actomyosin contractility in fibroblast-driven cancer invasion. *British journal of  
 613 cancer* 102, 392-402. 10.1038/sj.bjc.6605469.
- 614 12. Zeltz, C., Primac, I., Erusappan, P., Alam, J., Noel, A., and Gullberg, D. (2020). Cancer-associated  
 615 fibroblasts in desmoplastic tumors: emerging role of integrins. *Seminars in cancer biology* 62, 166-  
 616 181. 10.1016/j.semcancer.2019.08.004.
- 617 13. Goetz, J.G., Minguet, S., Navarro-Lerida, I., Lazcano, J.J., Samaniego, R., Calvo, E., Tello, M., Ostes-  
 618 Ibanez, T., Pellinen, T., Echarri, A., Cerezo, A., et al. (2011). Biomechanical remodeling of the  
 619 microenvironment by stromal caveolin-1 favors tumor invasion and metastasis. *Cell* 146, 148-163.  
 620 10.1016/j.cell.2011.05.040.
- 621 14. Tan, Y., Luo, X., Lv, W., Hu, W., Zhao, C., Xiong, M., Yi, Y., Wang, D., Wang, Y., Wang, H., Wu, Y., et al.  
 622 (2021). Tumor-derived exosomal components: the multifaceted roles and mechanisms in breast  
 623 cancer metastasis. *Cell death & disease* 12, 547. 10.1038/s41419-021-03825-2.
- 624 15. Al-Nedawi, K., Meehan, B., Micallef, J., Lhotak, V., May, L., Guha, A., and Rak, J. (2008). Intercellular  
 625 transfer of the oncogenic receptor EGFRvIII by microvesicles derived from tumour cells. *Nature cell  
 626 biology* 10, 619-624. 10.1038/ncb1725.

- 628 16. Skog, J., Wurdinger, T., van Rijn, S., Meijer, D.H., Gainche, L., Sena-Esteves, M., Curry, W.T., Jr., Carter,  
 629 B.S., Krichevsky, A.M., and Breakefield, X.O. (2008). Glioblastoma microvesicles transport RNA and  
 630 proteins that promote tumour growth and provide diagnostic biomarkers. *Nature cell biology* 10,  
 631 1470-1476. 10.1038/ncb1800.
- 632 17. Yu, D.D., Wu, Y., Shen, H.Y., Lv, M.M., Chen, W.X., Zhang, X.H., Zhong, S.L., Tang, J.H., and Zhao, J.H.  
 633 (2015). Exosomes in development, metastasis and drug resistance of breast cancer. *Cancer science*  
 634 106, 959-964. 10.1111/cas.12715.
- 635 18. Giordano, C., La Camera, G., Gelsomino, L., Barone, I., Bonofiglio, D., Ando, S., and Catalano, S. (2020).  
 636 The Biology of Exosomes in Breast Cancer Progression: Dissemination, Immune Evasion and  
 637 Metastatic Colonization. *Cancers* 12. 10.3390/cancers12082179.
- 638 19. Lee, Y.S., and Dutta, A. (2009). MicroRNAs in cancer. *Annual review of pathology* 4, 199-227.  
 639 10.1146/annurev.pathol.4.110807.092222.
- 640 20. Iorio, M.V., and Croce, C.M. (2012). MicroRNA dysregulation in cancer: diagnostics, monitoring and  
 641 therapeutics. A comprehensive review. *EMBO molecular medicine* 4, 143-159.  
 642 10.1002/emmm.201100209.
- 643 21. Rupaimoole, R., and Slack, F.J. (2017). MicroRNA therapeutics: towards a new era for the  
 644 management of cancer and other diseases. *Nature reviews. Drug discovery* 16, 203-222.  
 645 10.1038/nrd.2016.246.
- 646 22. Palma, F., Affinito, A., Nuzzo, S., Roscigno, G., Scognamiglio, I., Ingenito, F., Martinez, L., Franzese,  
 647 M., Zanfardino, M., Soricelli, A., Fiorelli, A., et al. (2021). miR-34c-3p targets CDK1 a synthetic lethality  
 648 partner of KRAS in non-small cell lung cancer. *Cancer gene therapy* 28, 413-426. 10.1038/s41417-  
 649 020-00224-1.
- 650 23. Silen, W., Machen, T.E., and Forte, J.G. (1975). Acid-base balance in amphibian gastric mucosa. *The  
 651 American journal of physiology* 229, 721-730. 10.1152/ajplegacy.1975.229.3.721.
- 652 24. Siemens, H., Jackstadt, R., Hunten, S., Kaller, M., Menssen, A., Gotz, U., and Hermeking, H. (2011).  
 653 miR-34 and SNAIL form a double-negative feedback loop to regulate epithelial-mesenchymal  
 654 transitions. *Cell cycle* 10, 4256-4271. 10.4161/cc.10.24.18552.
- 655 25. Roy, S., Levi, E., Majumdar, A.P., and Sarkar, F.H. (2012). Expression of miR-34 is lost in colon cancer  
 656 which can be re-expressed by a novel agent CDF. *Journal of hematology & oncology* 5, 58.  
 657 10.1186/1756-8722-5-58.
- 658 26. Jiang, L., and Hermeking, H. (2017). miR-34a and miR-34b/c Suppress Intestinal Tumorigenesis.  
 659 *Cancer research* 77, 2746-2758. 10.1158/0008-5472.CAN-16-2183.
- 660 27. Liang, J., Li, Y., Daniels, G., Sfanos, K., De Marzo, A., Wei, J., Li, X., Chen, W., Wang, J., Zhong, X.,  
 661 Melamed, J., et al. (2015). LEF1 Targeting EMT in Prostate Cancer Invasion Is Regulated by miR-34a.  
 662 *Molecular cancer research : MCR* 13, 681-688. 10.1158/1541-7786.MCR-14-0503.
- 663 28. Zhang, L., Wang, L., Dong, D., Wang, Z., Ji, W., Yu, M., Zhang, F., Niu, R., and Zhou, Y. (2019). MiR-  
 664 34b/c-5p and the neurokinin-1 receptor regulate breast cancer cell proliferation and apoptosis. *Cell  
 665 proliferation* 52, e12527. 10.1111/cpr.12527.
- 666 29. Stahlhut, C., and Slack, F.J. (2015). Combinatorial Action of MicroRNAs let-7 and miR-34 Effectively  
 667 Synergizes with Erlotinib to Suppress Non-small Cell Lung Cancer Cell Proliferation. *Cell cycle* 14,  
 668 2171-2180. 10.1080/15384101.2014.1003008.
- 669 30. Hong, D.S., Kang, Y.K., Borad, M., Sachdev, J., Ejadi, S., Lim, H.Y., Brenner, A.J., Park, K., Lee, J.L., Kim,  
 670 T.Y., Shin, S., et al. (2020). Phase 1 study of MRX34, a liposomal miR-34a mimic, in patients with  
 671 advanced solid tumours. *British journal of cancer* 122, 1630-1637. 10.1038/s41416-020-0802-1.
- 672 31. Ingenito, F., Roscigno, G., Affinito, A., Nuzzo, S., Scognamiglio, I., Quintavalle, C., and Condorelli, G.  
 673 (2019). The Role of Exo-miRNAs in Cancer: A Focus on Therapeutic and Diagnostic Applications.  
 674 *International journal of molecular sciences* 20. 10.3390/ijms20194687.
- 675 32. Kotani, A., Ito, M., and Kudo, K. (2021). Non-coding RNAs and lipids mediate the function of  
 676 extracellular vesicles in cancer cross-talk. *Seminars in cancer biology*.  
 677 10.1016/j.semcan.2021.04.017.
- 678 33. Sanz-Moreno, V., Gaggioli, C., Yeo, M., Albrengues, J., Wallberg, F., Viros, A., Hooper, S., Mitter, R.,  
 679 Feral, C.C., Cook, M., Larkin, J., et al. (2011). ROCK and JAK1 signaling cooperate to control

- 680 actomyosin contractility in tumor cells and stroma. *Cancer cell* 20, 229-245.  
 681 10.1016/j.ccr.2011.06.018.
- 682 34. Gaggioli, C., Hooper, S., Hidalgo-Carcedo, C., Grosse, R., Marshall, J.F., Harrington, K., and Sahai, E. (2007). Fibroblast-led collective invasion of carcinoma cells with differing roles for RhoGTPases in leading and following cells. *Nature cell biology* 9, 1392-1400. 10.1038/ncb1658.
- 683 35. Yamaguchi, H., and Sakai, R. (2015). Direct Interaction between Carcinoma Cells and Cancer  
 684 Associated Fibroblasts for the Regulation of Cancer Invasion. *Cancers* 7, 2054-2062.  
 685 10.3390/cancers7040876.
- 686 36. Timpson, P., McGhee, E.J., Erami, Z., Nobis, M., Quinn, J.A., Edward, M., and Anderson, K.I. (2011).  
 687 Organotypic collagen I assay: a malleable platform to assess cell behaviour in a 3-dimensional  
 688 context. *Journal of visualized experiments : JoVE*, e3089. 10.3791/3089.
- 689 37. Villarroya-Beltri, C., Gutierrez-Vazquez, C., Sanchez-Cabo, F., Perez-Hernandez, D., Vazquez, J.,  
 690 Martin-Cofreces, N., Martinez-Herrera, D.J., Pascual-Montano, A., Mittelbrunn, M., and Sanchez-  
 691 Madrid, F. (2013). Sumoylated hnRNPA2B1 controls the sorting of miRNAs into exosomes through  
 692 binding to specific motifs. *Nature communications* 4, 2980. 10.1038/ncomms3980.
- 693 38. Sheng, Y., Qi, S., Hu, R., Zhao, J., Rui, W., Miao, Y., Ma, J., and Yang, Q. (2019). Identification of blood  
 694 microRNA alterations in patients with severe active alopecia areata. *Journal of cellular biochemistry*  
 695 120, 14421-14430. 10.1002/jcb.28700.
- 696 39. Maschler, S., Wirl, G., Spring, H., Bredow, D.V., Sordat, I., Beug, H., and Reichmann, E. (2005). Tumor  
 697 cell invasiveness correlates with changes in integrin expression and localization. *Oncogene* 24, 2032-  
 698 2041. 10.1038/sj.onc.1208423.
- 700 40. Jang, I., and Beningo, K.A. (2019). Integrins, CAFs and Mechanical Forces in the Progression of Cancer.  
 701 *Cancers* 11. 10.3390/cancers11050721.
- 702 41. Sheppard, D. (1996). Epithelial integrins. *BioEssays : news and reviews in molecular, cellular and*  
 703 *developmental biology* 18, 655-660. 10.1002/bies.950180809.
- 704 42. Kumaravel, S., Abbey, C.A., Bayless, K.J., and Chakraborty, S. (2020). The beta1-integrin plays a key  
 705 role in LEC invasion in an optimized 3-D collagen matrix model. *American journal of physiology. Cell*  
 706 *physiology* 319, C1045-C1058. 10.1152/ajpcell.00299.2020.
- 707 43. Eiro, N., Fernandez-Garcia, B., Vazquez, J., Del Casar, J.M., Gonzalez, L.O., and Vizoso, F.J. (2015). A  
 708 phenotype from tumor stroma based on the expression of metalloproteases and their inhibitors,  
 709 associated with prognosis in breast cancer. *Oncoimmunology* 4, e992222.  
 710 10.4161/2162402X.2014.992222.
- 711 44. Eck, S.M., Cote, A.L., Winkelman, W.D., and Brinckerhoff, C.E. (2009). CXCR4 and matrix  
 712 metalloproteinase-1 are elevated in breast carcinoma-associated fibroblasts and in normal  
 713 mammary fibroblasts exposed to factors secreted by breast cancer cells. *Molecular cancer research*  
 714 : MCR 7, 1033-1044. 10.1158/1541-7786.MCR-09-0015.
- 715 45. Ito, A., Nakajima, S., Sasaguri, Y., Nagase, H., and Mori, Y. (1995). Co-culture of human breast  
 716 adenocarcinoma MCF-7 cells and human dermal fibroblasts enhances the production of matrix  
 717 metalloproteinases 1, 2 and 3 in fibroblasts. *British journal of cancer* 71, 1039-1045.  
 718 10.1038/bjc.1995.200.
- 719 46. Katoh, K. (2020). FAK-Dependent Cell Motility and Cell Elongation. *Cells* 9. 10.3390/cells9010192.
- 720 47. Joshi, R.S., Kanugula, S.S., Sudhir, S., Pereira, M.P., Jain, S., and Aghi, M.K. (2021). The Role of Cancer-  
 721 Associated Fibroblasts in Tumor Progression. *Cancers* 13. 10.3390/cancers13061399.
- 722 48. Busch, S., Andersson, D., Bom, E., Walsh, C., Stahlberg, A., and Landberg, G. (2017). Cellular  
 723 organization and molecular differentiation model of breast cancer-associated fibroblasts. *Molecular*  
 724 *cancer* 16, 73. 10.1186/s12943-017-0642-7.
- 725 49. Martinez-Outschoorn, U.E., Lisanti, M.P., and Sotgia, F. (2014). Catabolic cancer-associated  
 726 fibroblasts transfer energy and biomass to anabolic cancer cells, fueling tumor growth. *Seminars in*  
 727 *cancer biology* 25, 47-60. 10.1016/j.semcaner.2014.01.005.
- 728 50. Sotgia, F., Martinez-Outschoorn, U.E., Pavlides, S., Howell, A., Pestell, R.G., and Lisanti, M.P. (2011).  
 729 Understanding the Warburg effect and the prognostic value of stromal caveolin-1 as a marker of a  
 730 lethal tumor microenvironment. *Breast cancer research : BCR* 13, 213. 10.1186/bcr2892.

- 732 51. Mercier, I., Casimiro, M.C., Wang, C., Rosenberg, A.L., Quong, J., Minkeu, A., Allen, K.G., Danilo, C.,  
 733 Sotgia, F., Bonuccelli, G., Jasmin, J.F., et al. (2008). Human breast cancer-associated fibroblasts (CAFs)  
 734 show caveolin-1 downregulation and RB tumor suppressor functional inactivation: Implications for  
 735 the response to hormonal therapy. *Cancer biology & therapy* 7, 1212-1225. 10.4161/cbt.7.8.6220.
- 736 52. Roscigno, G., Cirella, A., Affinito, A., Quintavalle, C., Scognamiglio, I., Palma, F., Ingenito, F., Nuzzo,  
 737 S., De Micco, F., Cucuru, A., Thomas, R., et al. (2020). miR-216a Acts as a Negative Regulator of  
 738 Breast Cancer by Modulating Stemness Properties and Tumor Microenvironment. *International*  
 739 *journal of molecular sciences* 21. 10.3390/ijms21072313.
- 740 53. Kim, J.E., Kim, B.G., Jang, Y., Kang, S., Lee, J.H., and Cho, N.H. (2020). The stromal loss of miR-4516  
 741 promotes the FOSL1-dependent proliferation and malignancy of triple negative breast cancer. *Cancer*  
 742 *letters* 469, 256-265. 10.1016/j.canlet.2019.10.039.
- 743 54. Wu, H.J., Hao, M., Yeo, S.K., and Guan, J.L. (2020). FAK signaling in cancer-associated fibroblasts  
 744 promotes breast cancer cell migration and metastasis by exosomal miRNAs-mediated intercellular  
 745 communication. *Oncogene* 39, 2539-2549. 10.1038/s41388-020-1162-2.
- 746 55. Baroni, S., Romero-Cordoba, S., Plantamura, I., Dugo, M., D'Ippolito, E., Cataldo, A., Cosentino, G.,  
 747 Angeloni, V., Rossini, A., Daidone, M.G., and Iorio, M.V. (2016). Exosome-mediated delivery of miR-9  
 748 induces cancer-associated fibroblast-like properties in human breast fibroblasts. *Cell death & disease*  
 749 7, e2312. 10.1038/cddis.2016.224.
- 750 56. Chen, B., Sang, Y., Song, X., Zhang, D., Wang, L., Zhao, W., Liang, Y., Zhang, N., and Yang, Q. (2021).  
 751 Exosomal miR-500a-5p derived from cancer-associated fibroblasts promotes breast cancer cell  
 752 proliferation and metastasis through targeting USP28. *Theranostics* 11, 3932-3947.  
 753 10.7150/thno.53412.
- 754 57. Dou, D., Ren, X., Han, M., Xu, X., Ge, X., Gu, Y., and Wang, X. (2020). Cancer-Associated Fibroblasts-  
 755 Derived Exosomes Suppress Immune Cell Function in Breast Cancer via the miR-92/PD-L1 Pathway.  
 756 *Frontiers in immunology* 11, 2026. 10.3389/fimmu.2020.02026.
- 757 58. Donnarumma, E., Fiore, D., Nappa, M., Roscigno, G., Adamo, A., Iaboni, M., Russo, V., Affinito, A.,  
 758 Puoti, I., Quintavalle, C., Rienzo, A., et al. (2017). Cancer-associated fibroblasts release exosomal  
 759 microRNAs that dictate an aggressive phenotype in breast cancer. *Oncotarget* 8, 19592-19608.  
 760 10.18632/oncotarget.14752.
- 761 59. Duchartre, Y., Kim, Y.M., and Kahn, M. (2016). The Wnt signaling pathway in cancer. *Critical reviews*  
 762 in oncology/hematology 99, 141-149. 10.1016/j.critrevonc.2015.12.005.
- 763 60. Yoshida, T., Sopko, N.A., Kates, M., Liu, X., Joice, G., McConkey, D.J., and Bivalacqua, T.J. (2018).  
 764 Three-dimensional organoid culture reveals involvement of Wnt/beta-catenin pathway in  
 765 proliferation of bladder cancer cells. *Oncotarget* 9, 11060-11070. 10.18632/oncotarget.24308.
- 766 61. Ediriweera, M.K., Tennekoon, K.H., and Samarakoon, S.R. (2019). Role of the PI3K/AKT/mTOR  
 767 signaling pathway in ovarian cancer: Biological and therapeutic significance. *Seminars in cancer*  
 768 *biology* 59, 147-160. 10.1016/j.semcan.2019.05.012.
- 769 62. Chen, Y., Wang, T., Du, J., Li, Y., Wang, X., Zhou, Y., Yu, X., Fan, W., Zhu, Q., Tong, X., and Wang, Y.  
 770 (2018). The Critical Role of PTEN/PI3K/AKT Signaling Pathway in Shikonin-Induced Apoptosis and  
 771 Proliferation Inhibition of Chronic Myeloid Leukemia. *Cellular physiology and biochemistry : international*  
 772 *journal of experimental cellular physiology, biochemistry, and pharmacology* 47, 981-  
 773 993. 10.1159/000490142.
- 774 63. Nagase, H., Visse, R., and Murphy, G. (2006). Structure and function of matrix metalloproteinases  
 775 and TIMPs. *Cardiovascular research* 69, 562-573. 10.1016/j.cardiores.2005.12.002.
- 776 64. Bianchini, G., Balko, J.M., Mayer, I.A., Sanders, M.E., and Gianni, L. (2016). Triple-negative breast  
 777 cancer: challenges and opportunities of a heterogeneous disease. *Nature reviews. Clinical oncology*  
 778 13, 674-690. 10.1038/nrclinonc.2016.66.
- 779 65. Yu, T., and Di, G. (2017). Role of tumor microenvironment in triple-negative breast cancer and its  
 780 prognostic significance. *Chinese journal of cancer research = Chung-kuo yen cheng yen chiu* 29, 237-  
 781 252. 10.21147/j.issn.1000-9604.2017.03.10.
- 782 66. Dong, X., Bai, X., Ni, J., Zhang, H., Duan, W., Graham, P., and Li, Y. (2020). Exosomes and breast cancer  
 783 drug resistance. *Cell death & disease* 11, 987. 10.1038/s41419-020-03189-z.

- 784 67. Tomaszik, B., Papis-Ubych, A., Stawiski, K., Fijuth, J., Kedzierawski, P., Sadowski, J., Stando, R., Bibik,  
 785 R., Graczyk, L., Latuszek, T., Rutkowski, T., et al. (2021). Serum MicroRNAs as Xerostomia Biomarkers  
 786 in Patients With Oropharyngeal Cancer Undergoing Radiation Therapy. International journal of  
 787 radiation oncology, biology, physics. 10.1016/j.ijrobp.2021.07.008.
- 788 68. Sur, D., Balacescu, L., Cainap, S.S., Visan, S., Pop, L., Burz, C., Havasi, A., Buiga, R., Cainap, C., Irimie,  
 789 A., and Balacescu, O. (2021). Predictive Efficacy of MiR-125b-5p, MiR-17-5p, and MiR-185-5p in Liver  
 790 Metastasis and Chemotherapy Response Among Advanced Stage Colorectal Cancer Patients.  
 791 Frontiers in oncology 11, 651380. 10.3389/fonc.2021.651380.
- 792 69. Sun, J., Zhao, J., Yang, Z., Zhou, Z., and Lu, P. (2021). Identification of gene signatures and potential  
 793 therapeutic targets for acquired chemotherapy resistance in gastric cancer patients. Journal of  
 794 gastrointestinal oncology 12, 407-422. 10.21037/jgo-21-81.
- 795 70. Matsui, D., Zaidi, A.H., Martin, S.A., Omstead, A.N., Kosovec, J.E., Huleihel, L., Saldin, L.T., DiCarlo, C.,  
 796 Silverman, J.F., Hoppo, T., Finley, G.G., et al. (2016). Primary tumor microRNA signature predicts  
 797 recurrence and survival in patients with locally advanced esophageal adenocarcinoma. Oncotarget  
 798 7, 81281-81291. 10.18632/oncotarget.12832.
- 799 71. Gao, P., Wang, D., Liu, M., Chen, S., Yang, Z., Zhang, J., Wang, H., Niu, Y., Wang, W., Yang, J., and Sun,  
 800 G. (2020). DNA methylation-mediated repression of exosomal miR-652-5p expression promotes  
 801 oesophageal squamous cell carcinoma aggressiveness by targeting PARG and VEGF pathways. PLoS  
 802 genetics 16, e1008592. 10.1371/journal.pgen.1008592.
- 803 72. Torii, C., Maishi, N., Kawamoto, T., Morimoto, M., Akiyama, K., Yoshioka, Y., Minami, T., Tsumita, T.,  
 804 Alam, M.T., Ochiya, T., Hida, Y., et al. (2021). miRNA-1246 in extracellular vesicles secreted from  
 805 metastatic tumor induces drug resistance in tumor endothelial cells. Scientific reports 11, 13502.  
 806 10.1038/s41598-021-92879-5.
- 807 73. Ueta, E., Tsutsumi, K., Kato, H., Matsushita, H., Shiraha, H., Fujii, M., Matsumoto, K., Horiguchi, S.,  
 808 and Okada, H. (2021). Extracellular vesicle-shuttled miRNAs as a diagnostic and prognostic biomarker  
 809 and their potential roles in gallbladder cancer patients. Scientific reports 11, 12298. 10.1038/s41598-  
 810 021-91804-0.
- 811 74. Chen, S., Fu, Z., Wen, S., Yang, X., Yu, C., Zhou, W., Lin, Y., and Lv, Y. (2021). Expression and Diagnostic  
 812 Value of miR-497 and miR-1246 in Hepatocellular Carcinoma. Frontiers in genetics 12, 666306.  
 813 10.3389/fgene.2021.666306.
- 814 75. Kruger, S., Abd Elmageed, Z.Y., Hawke, D.H., Worner, P.M., Jansen, D.A., Abdel-Mageed, A.B., Alt,  
 815 E.U., and Izadpanah, R. (2014). Molecular characterization of exosome-like vesicles from breast  
 816 cancer cells. BMC cancer 14, 44. 10.1186/1471-2407-14-44.

817

818

819

820

821

822

823

824

825

826  
 827                   **FIGURE LEGENDS**

828                   **Figure 1- MDA-MB-231 cell-derived exosomes: characterization and fibroblast up-take.**  
 829                   A) Graph of results from the Nanoparticle tracking analysis performed on MDA-MB-231 cell-  
 830                   derived exosomes. The peak (at 105nm) indicates the mean ratio of vesicle size and  
 831                   concentration derived from three measurements. B) Western blot showing the expression of  
 832                   exosome-specific markers (CD63, CD81, CD9, and Tsg101) in MDA-MB-231 cells and  
 833                   exosomes, and the absence of the endoplasmic reticulum protein Calnexin. C) Representative  
 834                   TEM images of exosomes from MDA-MB-231 cells (scale bar: 500nm). Yellow square  
 835                   indicates a larger magnification (Scale bar: 100nm). D) Immunofluorescence assay performed  
 836                   on NFs (pt. #1) incubated with MDA-MB231 cell-derived exosomes labeled with PKH26 dye.  
 837                   The images from confocal microscopy show co-localization of the red signal derived from  
 838                   PKH26-labeled exosomes and the green signal from FITC-conjugated anti-β-Actin (Merged),  
 839                   indicative of exosome uptake by NFs. Magnification 63x.

840  
 841                   **Figure 2- MDA-MB-231 cell-derived exosomes promote a CAF-like phenotype in NFs.** A)  
 842                   Collagen contraction assay. Representative pictures of collagen plugs containing NFs cultured  
 843                   with MB-231 cell-derived exosomes (+Exosomes) or PBS (not treated, NT) after 24h. B)  
 844                   Histogram of mean collagen plug areas for NFs +Exosomes over NT measured with ImageJ.  
 845                   Standard deviations were calculated on replicates from two independent experiments performed  
 846                   with three different NF cell lines (pt. #1, #2, #3). P-value was calculated using the two-tailed  
 847                   unpaired t-test, \*\* p=0.0028. C) Migration assay performed with NFs (pt. #1, #2, #3) cultured  
 848                   in the presence of MDA-MB-231 cell-derived exosomes for 48h (+Exosomes) or PBS (NT).  
 849                   Representative bright-field images of NFs migrated through the Transwell® chamber and  
 850                   colored with crystal violet. Bars indicate size expressed in µm (pt. #2, #3) or pixels (pt. #1).  
 851                   Magnification 5x. D) Histogram of mean absorbance of crystal violet eluted from NFs  
 852                   +Exosomes over NT. Standard deviations were calculated on replicates from two independent  
 853                   experiments performed on three different NF cell lines (pt.#1, #2, #3). P-value was calculated  
 854                   using the two-tailed unpaired t-test, \* p=0.039. E) Histogram of quantitative real time-PCR  
 855                   showing FAP, Caveolin-1, SLC16A3, and SLC2A1 mRNAs relative expression in NFs  
 856                   +Exosomes over NT. Standard deviations were calculated on replicates from two independent  
 857                   experiments performed on three different NF cell lines (pt. #1, #2, #3). P-value was calculated  
 858                   using the multiple t-test with FDR adjustment (FAP and SLC2A1\*\* p=0.0014; SLC16A3  
 859                   \*\*\*=0.00064; Caveolin-1\*\*\* p=0.00014).

860

861 **Figure 3- 3D Organotypic invasion assay of normal breast epithelial cells in a matrix**  
 862 **containing exosome-activated fibroblasts.** A) Left panel: representative phase contrast images  
 863 of collagen matrix embedded section (10 $\mu$ m slides) showing MCF10A cell invasion through  
 864 the matrix when three-dimensional co-cultured with NFs (pt.#3) incubated with MDA-MB-  
 865 231-derived exosomes (+Exosomes) or PBS (NT). Right panel: confocal microscopy images  
 866 of collagen matrix sections showing MCF10A cells stained with DAPI for nuclei (blue signal)  
 867 and ALEXA594-conjugated anti-Pan-cytokeratin antibody (red signal) as epithelial marker. B)  
 868 Histogram of the number of invading MCF10A (NF + Exosomes and NF\_NT) calculated in  
 869 different fields of confocal microscopy images. Standard deviations were calculated on technical  
 870 replicates. P-values were calculated using two-tailed unpaired t test; \*\*\*p<0.0001.

871

872 **Figure 4- Differentially expressed miRNAs in fibroblasts upon exposure to MDA-MB-231**  
 873 **cell-derived exosomes.** A) Heatmap of data from small-RNA sequencing analysis showing  
 874 miRNAs differentially expressed in NFs (pt. #1) incubated with MDA-MB-231 cell-derived  
 875 exosomes (+Exosomes) and PBS (NT). Upregulated miRNAs represented in green,  
 876 downregulated miRNAs in red. The results are based on technical duplicates (p-value < 0.05).  
 877 B) Histograms of q-RT-PCR results showing the expression levels of miR-185-5p, -652-5p,  
 878 and miR-1246 in NFs (pt.#1) incubated with Exosomes compared to NT. Data are showed  
 879 as the relative expression of the miRs. Standard deviations were calculated on technical  
 880 duplicates. P-value was calculated using unpaired t-test (\*p= 0,0317; \*\*\*p= 0,0008). C)  
 881 Histograms of q-RT-PCR results showing the basal expression levels of miR-185-5p, -652-5p,  
 882 and miR-1246 in NFs as compared to CAFs. Data are shown as relative expression of miRs  
 883 folded on NFs. Standard deviations were calculated replicates from two independent  
 884 experiments performed on four different primary NF cell lines (pt. #1, #2, #3, and #4) and  
 885 four different primary CAF cell lines (pt.#81, #82, #87, and #89). P-value was calculated  
 886 with unpaired t-test (\*p= 0,0210; \*\*p= 0,0027). D) Representative images of the Exomotif  
 887 analysis with MDS<sup>2</sup> software showing short motif (3 to 5 nucleotides) contained in miR-185-  
 888 5p, -652-5p, and miR-1246 sequences and predictive of their active loading into exosomes.  
 889 E) Western blot showing the overexpression of FAP, Caveolin-1, and MCT4 proteins in NFs  
 890 (pt. #1, #2, #3) transfected with combo miRs as compared to control (Scra) after 72h. F)  
 891 Histogram of densitometric measurement of bands, obtained with ImageJ. Quantification of  
 892 protein expression is represented as the mean of folded densitometry from NFs transfected  
 893 with combo miRs over Scra. Standard deviations were calculated on replicates from two

894 independent experiments performed on three different NF cell lines (pt. #1, #2, #3). P-value  
 895 was calculated using the multiple t-test with FDR adjustment (FAP \*\*\*p<0.0001; MCT4 \*\*  
 896 p=0.0019; Caveolin-1\*\*p=0.0016).

897

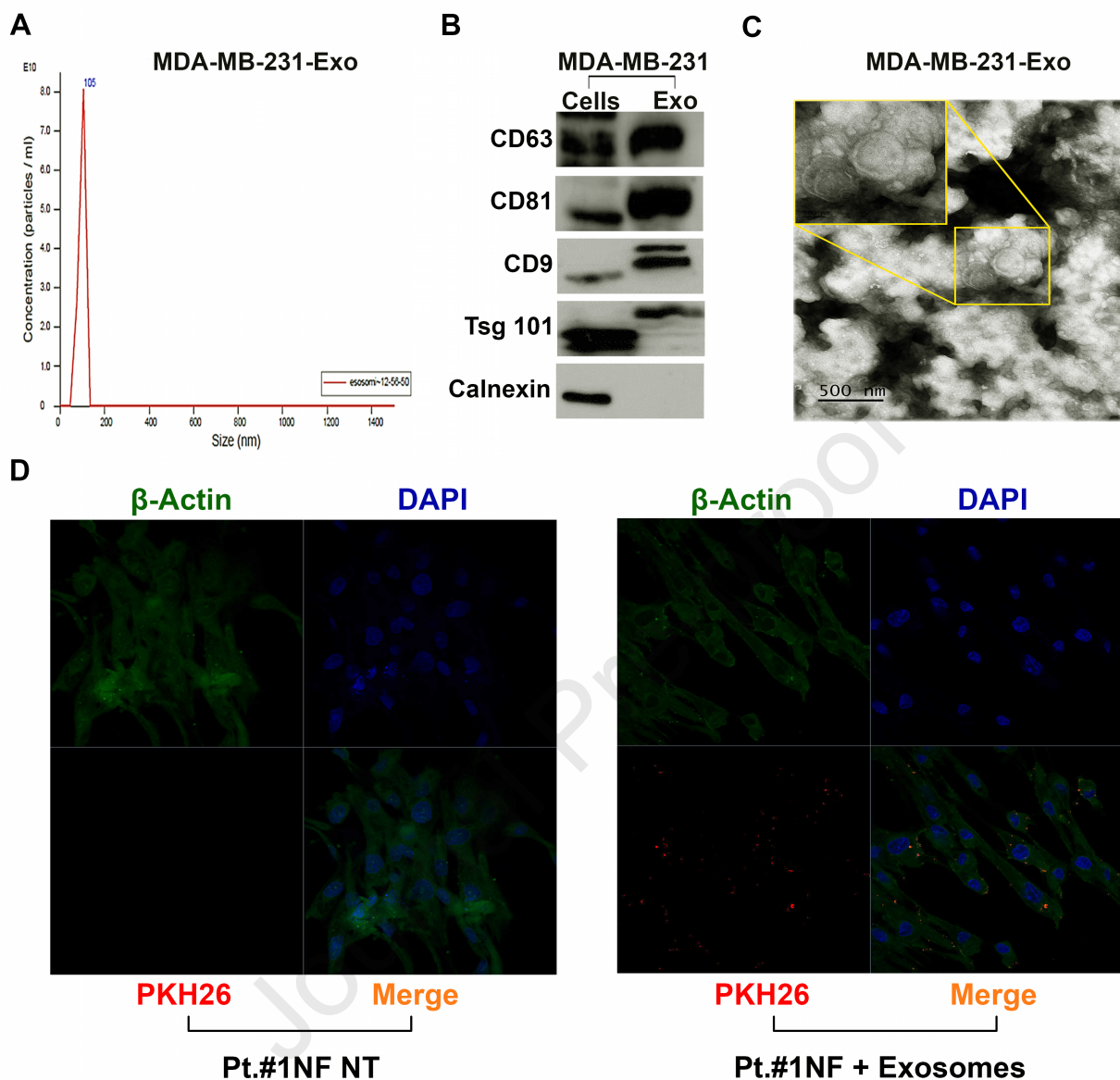
898 **Figure 5- Combo miRs promote fibroblast-mediated ECM remodeling.** A) Representative  
 899 pictures of collagen plugs containing NFs transfected with combo miRs or Scra taken after  
 900 24h. B) Histogram of mean collagen plug area for NFs transfected with combo miRs, fold  
 901 over Scra at 24h (ImageJ). Standard deviations were calculated on replicates from two  
 902 independent experiments performed with three different NF cell lines (pt. #1, #2, #3). P-value  
 903 was calculated using the two-tailed unpaired t-test; \*\* p=0.0011. C) Transwell invasion assay  
 904 with NFs (pt. #2, #3) transfected with combo miRs or Scra (control). Representative bright  
 905 field images of NFs that invaded the matrix and migrated through the Transwell chamber  
 906 fixed and colored with crystal violet. Bars indicate size, expressed in  $\mu\text{m}$  or px. Magnification  
 907 5x. D) Histogram of mean absorbance values for crystal violet eluted from NFs transfected  
 908 with combo miRs folded on Scra. Standard deviations were calculated on replicates from two  
 909 independent experiments performed on two different NF cell lines (pt. #2, #3). P-value was  
 910 calculated using the two-tailed unpaired t-test, \*\* p=0.0018. E) Western blot showing  
 911 overexpression of MMP1, MMP2, and MMP3 proteins together with ITGB1 and ITGA5 in  
 912 NFs (pt. #1, #2, #3) transfected with combo miRs and Scra after 48h and 72h. F) Histograms  
 913 of mean densitometric measurement of bands (ImageJ) for NFs transfected with combo miRs  
 914 over Scra. Standard deviations were calculated on replicates from two independent experiments  
 915 performed on three different NF cell lines (pt. #1, #2, #3). P-value was calculated using  
 916 multiple t-test with FDR adjustment (MMP1\* p=0.023; MMP2\*\*\* p=0.00087;  
 917 MMP3\*\*p=0.0035; ITGB1\*\*\*p=0.00014; ITGA5 \*\*p=0.0054).

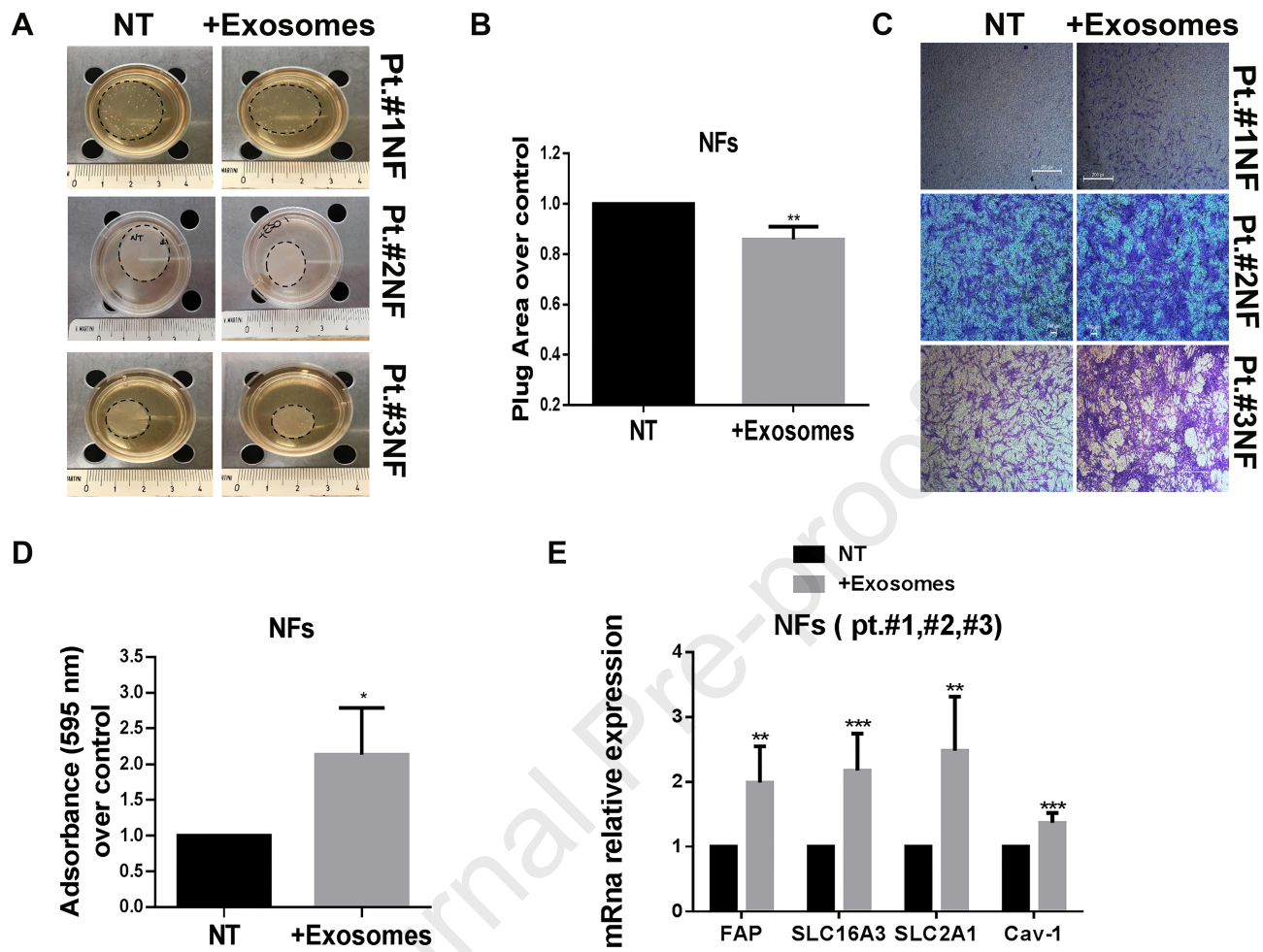
918

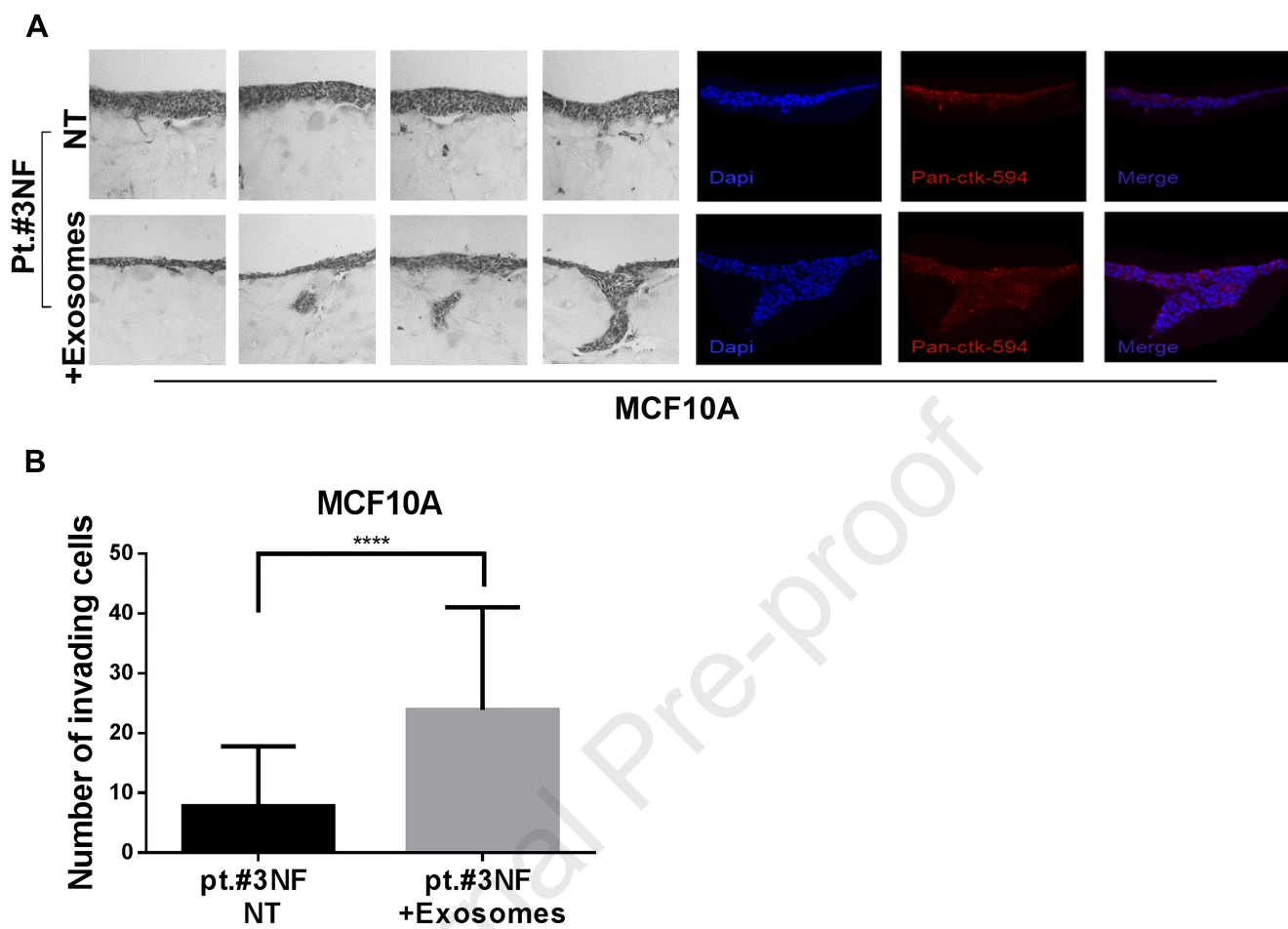
919 **Figure 6- Combo miRs promote migration of NFs.** A) Wound healing assay performed  
 920 with NFs transfected with combo miRs or Scra. Representative images in bright field of NFs  
 921 at 0h and 24h from the scratch. Bars indicate size, expressed in pixels (px). B) Histogram  
 922 of mean scratch area at 24h, normalized on 0h of NFs transfected with combo miRs over  
 923 Scra. Standard deviations were calculated on replicates from two independent experiments  
 924 performed on three different NF cell lines (pt. #1, #2, #3). P-value was calculated using the  
 925 two-tailed unpaired t-test, \*\* p=0.0061. C) Transwell migration assay performed with NFs  
 926 (pt. #1, #2, #3) transfected with combo miRs and Scra (control). Representative images in

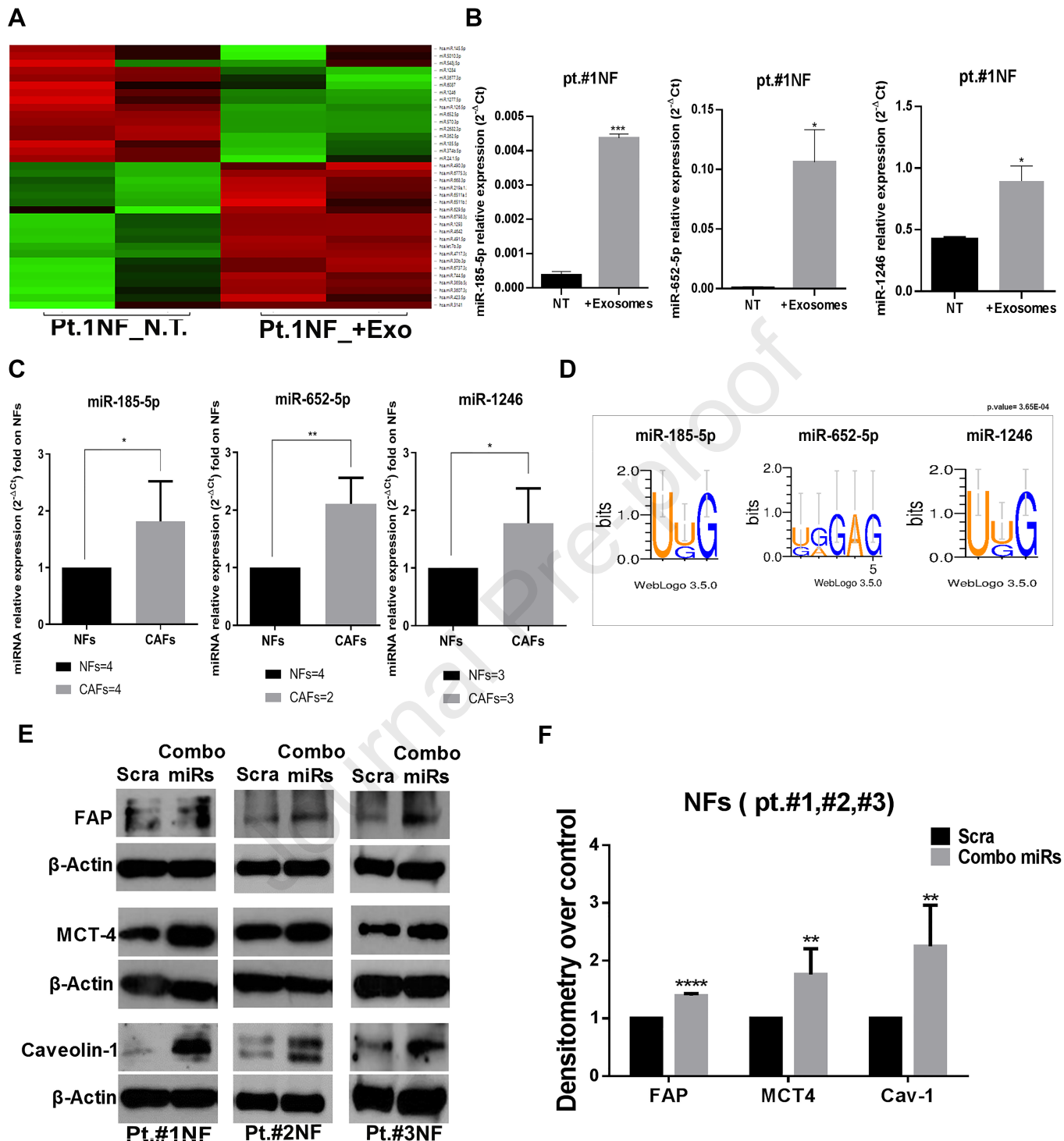
927 bright field of NFs migrating through the Transwell chamber and colored with crystal violet.  
928 Bars on the images indicate size, expressed in  $\mu\text{m}$  (pt. #1, #2) or pixels (pt. #3). D)  
929 Histogram of mean absorbance values of crystal violet eluted from migrated cells. Standard  
930 deviations were calculated on replicates from two independent experiments performed on three  
931 different NF cell lines (pt. #1, #2, #3). P-value was calculated using the two-tailed unpaired  
932 t-test, \*\* p=0.0049. E) Western blot showing overexpression of phosphorylated FAK  
933 (Y576/577) protein in NFs transfected with combo miRs compared to Scra after 72h. F)  
934 Histogram of mean densitometric measurement of bands (ImageJ) for NFs transfected with  
935 combo miRs over Scra. Standard deviations were calculated on replicates from two independent  
936 experiments performed on three different NF cell lines (pt. #1, #2, #3). P-value was calculated  
937 using the two-tailed unpaired t-test, \* p=0.029.

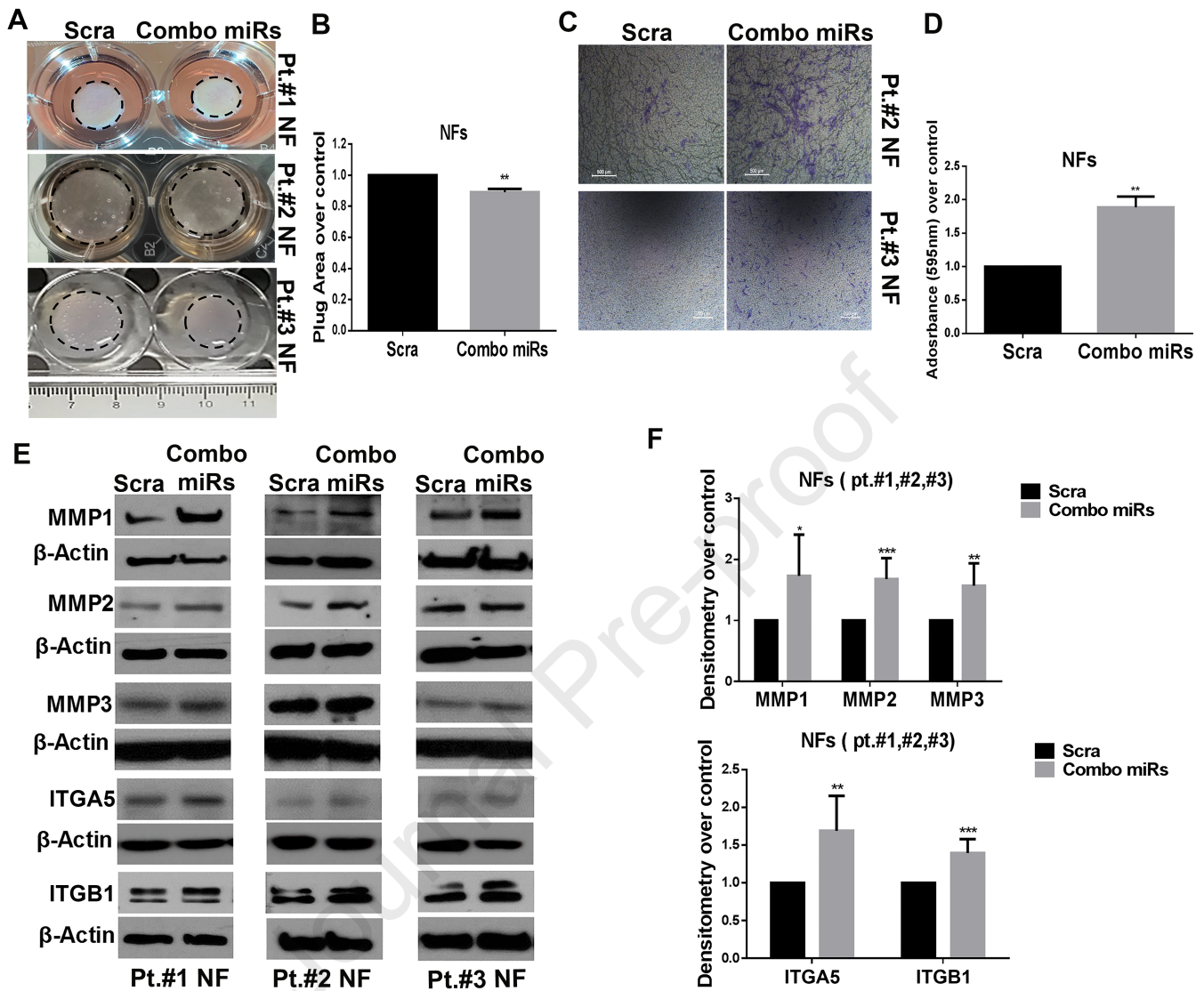
938

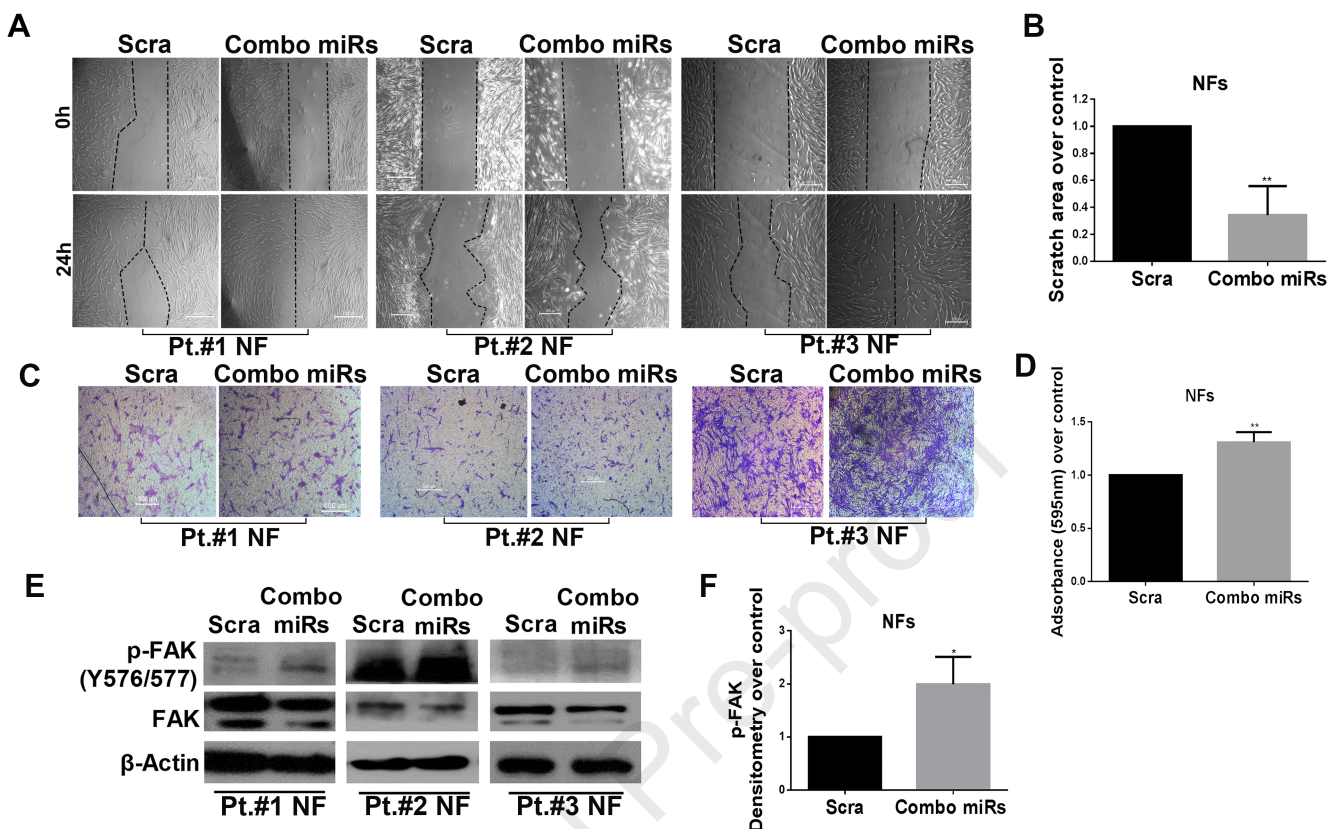












**eTOC synopsis**

Study of mechanisms involved in the crosstalk between breast cancer cells and stromal fibroblasts in the tumor microenvironment context. Identification of microRNAs from breast cancer cell-derived exosomes able to synergistically activate stromal fibroblasts towards cancer-associated fibroblasts-related pro-migratory phenotype.